Mechanical overstimulation causes acute injury and synapse loss followed by fast recovery in lateral-line neuromasts of larval zebrafish

Melanie Holmgren[1], Michael E. Ravicz[4,5], Kenneth E. Hancock[4,5], Olga Strelkova[4,5], Artur A. Indzhykulian[4,5], Mark E. Warchol[1,3], Lavinia Sheets[1,2]*

1. Department of Otolaryngology, Washington University School of Medicine, St. Louis, MO, USA
2. Department of Developmental Biology, Washington University School of Medicine, St. Louis, MO, USA
3. Department of Neuroscience, Washington University School of Medicine, St. Louis, MO, USA
4. Eaton-Peabody Laboratory, Massachusetts Eye and Ear, Boston, Massachusetts, USA
5. Department of Otolaryngology–Head and Neck Surgery, Harvard Medical School, Boston, Massachusetts, USA

*** Corresponding author**
Lavinia Sheets: sheetsl@wustl.edu

Abstract

Excess noise damages sensory hair cells, resulting in loss of synaptic connections with auditory nerves and hair-cell death. The cellular mechanisms underlying mechanically induced hair-cell damage and subsequent repair are not completely understood. Hair cells in neuromasts of larval zebrafish are structurally and functionally comparable to mammalian hair cells but undergo robust regeneration following damage. We therefore developed a model for mechanically induced hair-cell damage in this highly tractable system. Free swimming larvae exposed to strong water current for 2 hours displayed mechanical injury to neuromasts, including afferent neurite retraction, damaged hair bundles, and reduced mechanotransduction. Synapse loss was observed in apparently intact exposed neuromasts, and this loss was exacerbated by inhibiting glutamate uptake. Mechanical damage also elicited an inflammatory response and macrophage recruitment. Remarkably, neuromast morphology, synapse number, and hair-cell function fully recovered within 2 days following exposure. Our results indicate functional changes and synapse loss in mechanically damaged lateral-line neuromasts that appear similar to damage observed in noise-exposed mammalian ear yet are completely repaired.

Keywords: Hair cell, mechanical damage, ribbon synapse, inflammation, regeneration

36

37 Introduction

38 Hair cells are the sensory receptors of the inner ear and lateral-line organs that detect
39 sound, orientation, and motion. They transduce these stimuli through deflection of stereocilia,
40 which opens mechanically-gated cation channels (LeMasurier & Gillespie, 2005; Qiu & Muller,
41 2018) and drives subsequent transmission of sensory information via excitatory glutamatergic
42 synapses (Glowatzki & Fuchs, 2002). Excessive mechanical stimulation, such as loud noise,
43 can damage hair cells and their synaptic connections to afferent nerves. The degree of damage
44 depends on the intensity and duration of the stimulus, with higher levels of traumatic noise
45 leading to hair-cell loss (Cho et al., 2013; Nordmann, Bohne, & Harding, 2000) and lower levels
46 leading to various pathologies, including damage to the hair-cell mechanotransduction
47 complex/machinery and stereocilia (Gao, Ding, Zheng, Ruan, & Liu, 1992; Husbands,
48 Steinberg, Kurian, & Saunders, 1999), misshapen hair cells (Bullen, Anderson, Bakay, & Forge,
49 2019), synaptic terminal damage, neurite retraction, and hair-cell synapse loss (Fernandez et
50 al., 2020; Henry & Mulroy, 1995; Kujawa & Liberman, 2009; Puel, Ruel, Gervais d'Aldin, & Pujol,
51 1998). In addition to directly damaging hair cells, excess noise also initiates an inflammatory
52 response (Hirose, Discolo, Keasler, & Ransohoff, 2005; Kaur et al., 2019). Such inflammation is
53 mediated by macrophages, a class of leukocyte that responds to injury by clearing cellular
54 debris and promoting tissue repair (Wynn & Vannella, 2016).

55 The variety of injury and range of severity suggests multiple signaling pathways are
56 involved in hair-cell damage associated with exposure to strong mechanical stimuli. Also
57 unknown are the cellular processes mediating repair following such trauma. While hair cells
58 show a partial capacity for repair of stereocilia and synaptic connections, some sub-lethal
59 damage to hair cells is permanent. Numerous studies of the mammalian cochlea suggest that a
60 subgroup of inner hair-cell synapses are permanently lost following noise exposure (Cho et al.,
61 2013; Hickman, Smalt, Bobrow, Quatieri, & Liberman, 2018; Kujawa & Liberman, 2009; Shi et
62 al., 2013). Glutamate excitotoxicity is likely the pathological event that initiates noise-induced
63 hair-cell synapse loss (Hu, Rutherford, & Green, 2020; Kim et al., 2019; Puel et al., 1998), but
64 the downstream cellular mechanisms are still undefined. Further, the cellular mechanisms that
65 promote hair-cell synapse recovery following damage-induced loss are also not understood.

66 Zebrafish have proven to be a valuable model system for studying the molecular basis of
67 hair-cell injury and repair. Zebrafish sensory hair cells are structurally and functionally
68 homologous to mammalian hair cells (Coffin, Kelley, Manley, & Popper, 2004; Kindt & Sheets,
69 2018; Sebe et al., 2017). In contrast to other vertebrate model organisms, zebrafish hair cells

70 are optically accessible in whole larvae within the lateral-line organs. These sensory organs,
71 called neuromasts, contain clusters of ~ 14 hair cells each and are distributed throughout the
72 external surface of the fish to detect local water movements. Zebrafish can regenerate complex
73 tissues, including lateral-line organs (Kniss, Jiang, & Piotrowski, 2016; Xiao et al., 2015). This
74 capacity for organ repair combined with optical accessibility allows us to study cellular and
75 synaptic damage and repair *in vivo* following mechanical trauma.
76 In order to model mechanical damage in zebrafish lateral-line organs, we developed a
77 protocol to mechanically stimulate the lateral line of free-swimming 7-day-old larvae. Using this
78 protocol, we were able to induce mechanical injury to lateral-line organs that resembled the
79 trauma observed in the mammalian cochlea following acoustic overstimulation. We observed
80 synapse loss and enlargement of postsynaptic densities (PSDs) in all exposed neuromasts as
81 well as hair-cell loss and afferent neurite retraction in a subset of neuromasts. Hair cell
82 mechanotransduction, as measured by uptake of the cationic dye FM1-43, was significantly
83 reduced after mechanical injury. We also observed an inflammatory response similar to that
84 observed in the mammalian cochlea after noise trauma. Remarkably, mechanically induced
85 lateral-line damage appeared to rapidly recover; hair-cell number and morphology returned to
86 normal within 4 - 8 hours following exposure, concurrent with clearance of cellular debris by
87 macrophages. Additionally, neuromasts showed partial recovery of afferent innervation, FM1-43
88 uptake, and hair-cell synapse number within 2 hours following exposure, and completely
89 recovered by 2 days post-exposure, indicating mechanically injured neuromasts fully repair
90 following damage.

91 Results

92 **Mechanical overstimulation of zebrafish lateral-line hair cells**

93 To mechanically damage hair cells of lateral-line organs in free-swimming 7-day-old
94 zebrafish, we developed a stimulation protocol using an electrodynamic shaker to create a
95 strong water current (Fig.1 A). The frequency used for mechanical stimulation was selected and
96 further verified (see Method Details) based on previous studies showing 60 Hz to be within the
97 optimal upper frequency range of mechanical sensitivity of superficial posterior lateral-line
98 neuromasts (which respond maximally between 10-60 Hz), but a suboptimal frequency for hair
99 cells of the anterior macula of the inner ear (Levi, Akanyeti, Ballo, & Liao, 2015; Trapani &
100 Nicolson, 2010; Weeg, Fay, & Bass, 2002). Dorsal-ventral displacement of a 6-well dish at 60
101 Hz and acceleration of 40.3 m/s^2 (+/-0.5m/s^2) created water flow and disturbance of the water
102 surface that was strong enough to trigger 'fast start' escape responses—a behavior mediated in

103 part by zebrafish lateral-line organs to escape predation (Fig. 1 B inset) (McHenry, Feitl,

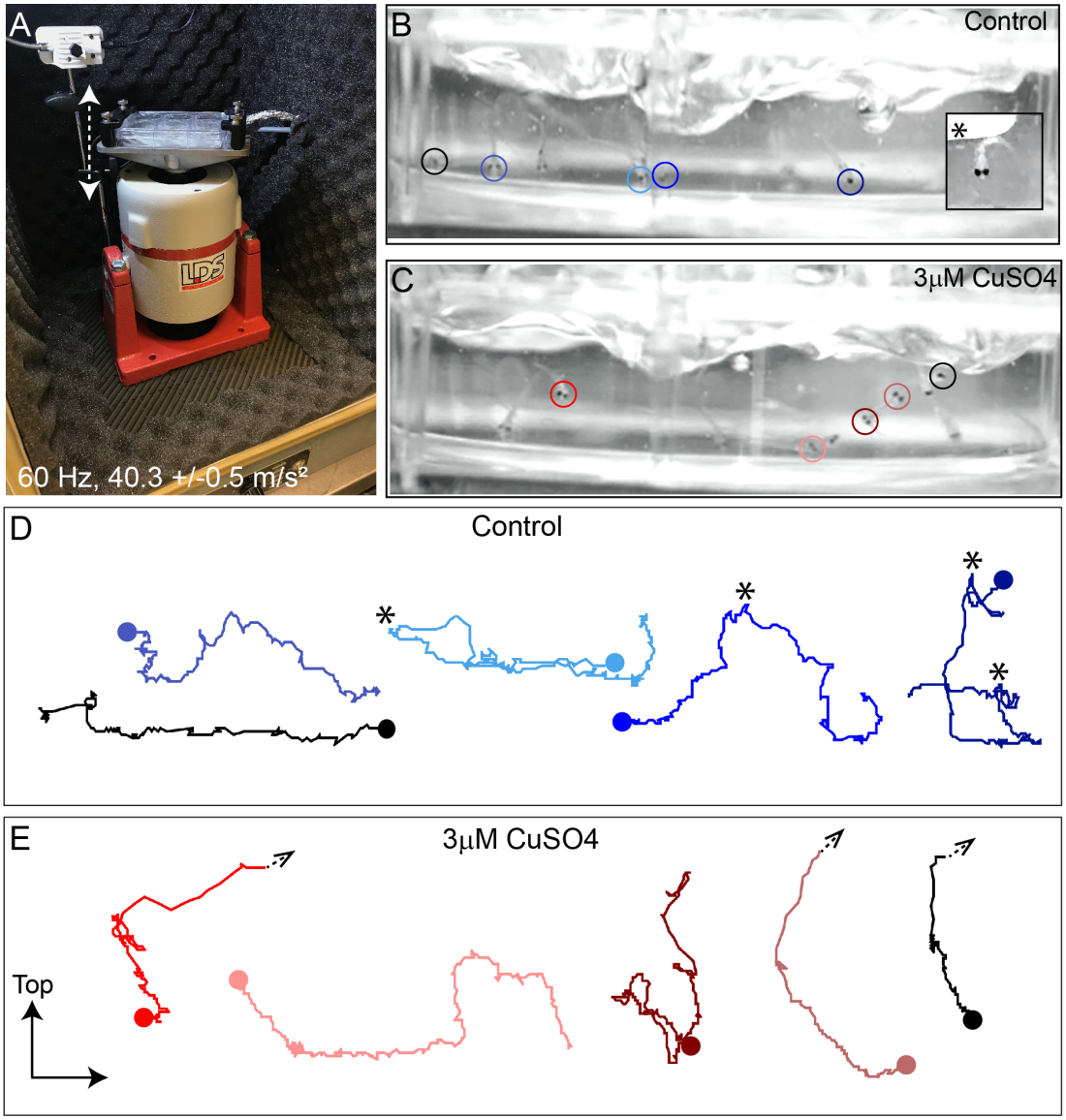

Figure 1: Intense current produced by shaker apparatus stimulates lateral-line hair cells and evokes a relevant behavior response. **(A)** The apparatus: a magnesium head expander holding a 6-well dish mounted on a vertically oriented electrodynamic shaker housed inside a sound-attenuation chamber. The stimulus consisted of a 60 Hz vertical displacement of the plate (hatched arrows) driven by an amplifier and controlled by a modified version of the Eaton-Peabody Laboratory Cochlear Function Test Suite. **(B,D)** Swimming behavior of 7-day-old larvae during exposure to the wave stimulus. Traces in (D) represent tracking of corresponding circled fish over 500 ms (1000 fps/ 500 frames). Asterisks indicate a "fast escape" response (B; inset). **(C,E)** Swimming behavior of larvae whose lateral-line neuromasts were ablated with low-dose $CuSO_4$. Arrows in (E) indicate where a larva was swept into the waves and could no longer be tracked

104 Strother, & Van Trump, 2009; Nair, Azatian, & McHenry, 2015). 'Fast start' escape responses
105 can be activated by stimulating hair cells of the lateral line and/or the posterior macula in the ear
106 (Bhandiwad, Zeddies, Raible, Rubel, & Sisneros, 2013). To verify that the observed escape
107 responses were mediated predominantly by flow sensed by lateral-line hair cells rather than hair

108 cells of the macula, we exposed a group of larvae to low dose (3μM) copper sulfate ($CuSO_4$) for
109 1 hour to specifically ablate lateral-line hair cells, but leave hair cells of the ear intact (Olivari,
110 Hernandez, & Allende, 2008). Following a 2 hr recovery after $CuSO_4$ treatment, we recorded
111 fish behavior with a high-speed camera during the stimulus (1000 fps for 10 s) and compared
112 the responses of fish with lesioned lateral-line organs with those of untreated control siblings
113 (Fig. 1 B,C; Movie S1,2). When subjected to intense water flow, we found that 'fast start'
114 responses—defined as a c-bend of the body occurring within 15 ms followed by a counter-bend
115 (Burgess & Granato, 2007; McHenry et al., 2009)—occurred significantly less frequently in
116 larvae with ablated lateral line organs than in siblings with intact lateral line (Fig. 1 C,E; avg.
117 'fast start' responses: : 0.4 (± 0.1)/s in lateral-line ablated vs 1.5 (± 0.1)/s in control; 3 trials,10 s
118 per trial; **P=0.0043). Accordingly, some $CuSO_4$-treated fish were unable to escape the current
119 and were swept into the waves (Fig. 1 E; arrowheads; Movie S2). These observations indicate
120 that the strong current generated by our device is stimulating lateral-line hair cells and evoking a
121 behaviorally relevant response.

122 **A subset of mechanically injured neuromasts undergo physical displacement that is**
123 **position dependent but does not require mechanotransduction**

124 To induce mechanical damage to lateral line organs, larvae (10-15 per well) were
125 exposed to an initial 20 minutes of strong water current stimulus followed by 10 minutes of rest,
126 then 2 hours of continuous stimulus (Supplemental Fig. 1A). The ten-minute break in exposure
127 was introduced early on when establishing the stimulus duration because it appeared to
128 enhance larval survival; it was therefore maintained throughout the study for consistency. Fish
129 were euthanized and fixed immediately after exposure, then processed for
130 immunohistofluorescent labeling of hair cells and neurons. Unexposed sibling fish served as
131 controls. As posterior lateral-line (pLL) neuromasts have been shown to specifically initiate
132 escape behavior in response to strong stimuli (Liao & Haehnel, 2012), analysis of the
133 morphology of pLL neuromasts L3, L4, and L5 was conducted for exposed and control larvae
134 (Fig. 2 A). Initially, we divided the observed neuromast morphology into two categories:
135 "normal", in which hair cells were radially organized with a relatively uniform shape and size,
136 and "disrupted", in which the hair cells were misshapen and displaced to one side, with the
137 apical ends of the hair cells localized anteriorly (Fig. 2 B, C; see Methods Details for measurable
138 criteria). Position of the neuromast along the tail was also associated with vulnerability to
139 disruption; we observed a gradient of damage in the pLL from rostral to caudal i.e. L5 was more
140 susceptible to disruption than L4, which was more susceptible to disruption than L3 (Fig. 2 F;
141 Repeated measure One-way ANOVA *P=0.0386, **P=0.0049, ***= 0.0004).

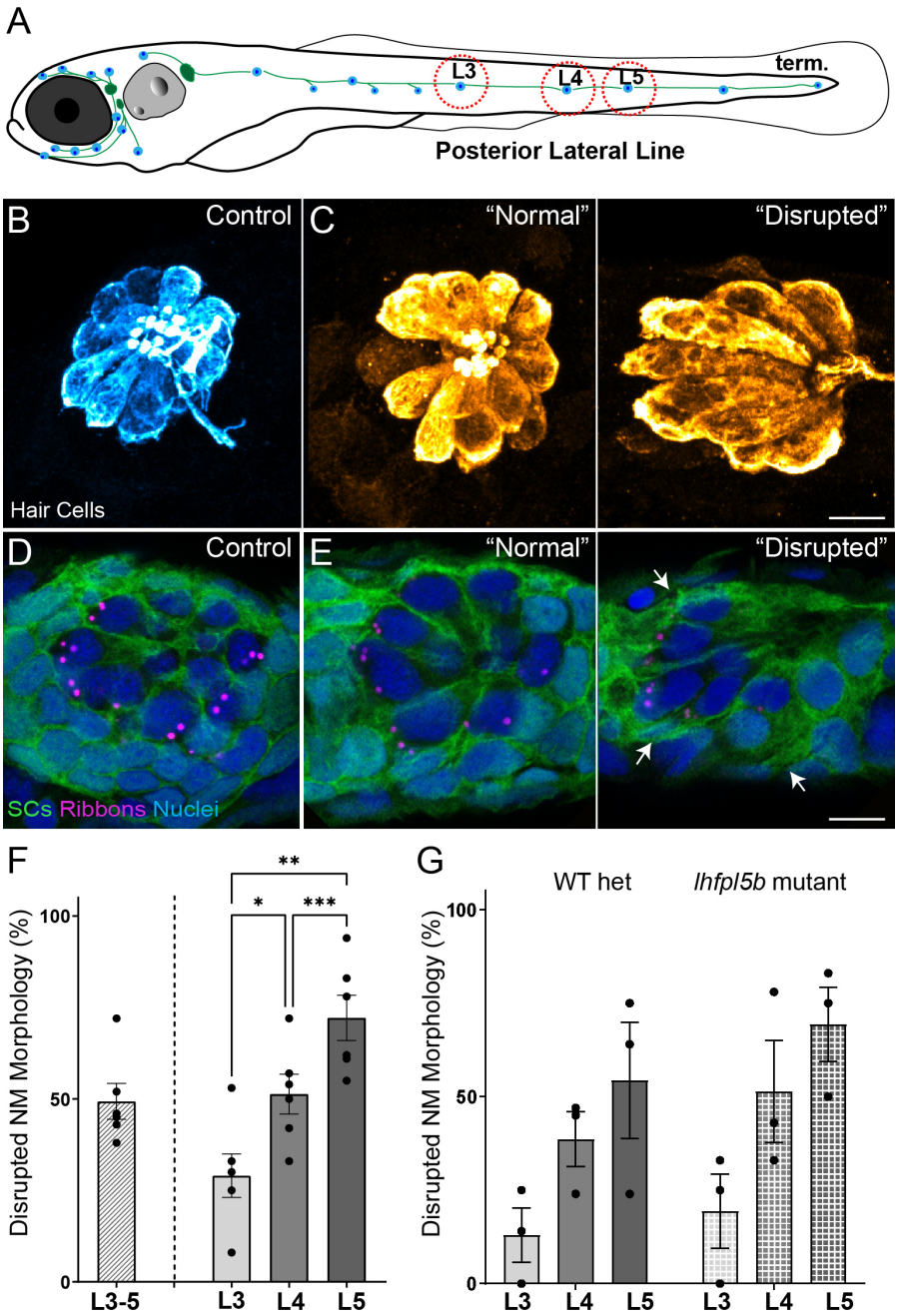

Figure 2: Morphological changes in pLL neuromast hair cells exposed to strong water current stimulus. **(A)** Schematic of a larval zebrafish. Blue dots indicate neuromasts of the lateral-line organs; green lines indicate innervating afferent lateral-line nerves. pLL neuromasts L3, L4, and L5 were analyzed (dashed circles). **(B-C)** Maximum intensity dorsal top-down 2D projections of confocal images of control (B) or stimulus-exposed (C) neuromast hair cells (blue or orange; Parvalbumin immunolabel). Exposed neuromast hair-cell morphology was categorized as "normal" i.e. radial hair-cell organization indistinguishable from control or "disrupted" i.e. asymmetric organization with the hair-cell apical ends oriented posteriorly. D) Maximum intensity projections of supporting cells expressing GFP (SC, green), immunolabeled synaptic ribbons (magenta; Ribeye b) and all cell nuclei (blue; DAPI). White arrows indicate displaced SCs. (Scale bars: 5μm). **(F)** Average percentage of neuromasts with "disrupted" morphology following mechanical stimulation. Each dot represents the percentage of disrupted neuromasts (NM) in a single experimental trial. Disrupted hair-cell morphology was place dependent, with neuromasts more frequently disrupted following sustained stimulus and when localized toward the posterior end of the tail (*P=0.0386, **P=0.0049, ***P=0.0004) **(G)** Average percentage of exposed neuromasts (NM) with "disrupted" morphology in *lhfpl5b* mutants, which lack mechanotransduction specifically in lateral-line hair cells, vs. heterozygous WT. *lhfpl5b* mutants show a similar gradient of neuromast disruption following mechanical injury as WT siblings. Error Bars = SEM

Additionally, we compared mechanical stress from our sustained exposure to an exposure protocol that delivered intermittent pulses of stimulus ("periodic exposure"; Supplemental Fig.1 A). We observed neuromast disruption less frequently with periodic exposures vs. sustained exposure of the same intensity (Supplemental Figure 1 B; Unpaired t-test **P=0.0034), supporting that displacement of neuromasts is a consequence of mechanical injury. Additionally,

149 we examined hair cell morphology in the ears of larvae exposed to sustained stimulus and
150 observed no apparent damage (Supplemental Fig. 2), indicating our overstimulation protocol
151 produces mechanical damage specifically to lateral-line organs.
152 To determine if hair-cell activity plays a role in the displacement of neuromasts, we
153 exposed *lhfpl5b* mutants—fish that have intact hair cell function in the ear, but no
154 mechanotransduction in hair cells of the lateral line—to sustained stimulation (Erickson,
155 Pacentine, Venuto, Clemens, & Nicolson, 2019). We observed comparable morphological
156 disruption of neuromasts lacking mechanotransduction (Fig. 2G), suggesting that displacement
157 of lateral-line hair cells is due to physical damage from the stimulus. Further, we observed the
158 adjacent supporting cells in neuromasts with disrupted hair-cell morphology appeared similarly
159 displaced and elongated (Fig. 2 E; white arrows), indicating that mechanical injury disrupts the
160 structural integrity of the entire neuromast organ.

161 **Hair-cell loss and loss of afferent nerve contacts correspond to neuromast disruption**

162 Moderate noise exposures can cause damage or loss of cochlear hair-cell synapses,
163 including swelling and retraction of afferent nerve fibers, while more extended and/or severe
164 exposures lead to hair-cell loss. To address whether mechanical damage in the lateral line
165 produced similar morphological changes, we surveyed the number of hair cells per neuromast
166 and the percentage of neuromast hair cells lacking afferent innervation in fish immediately
167 following exposure to sustained stimulation (Fig. 3). We observed a reduction in the number of
168 hair cells per neuromast immediately following exposure (Fig. 3 D; Unpaired t-test, *P=0.0125;
169 n=114-149 L3-L5 neuromasts; N=13 trials) as well as a significant reduction in the percentage
170 of hair cells per neuromast innervated by afferent neurons (Fig. 3 E; One sample Wilcoxon test,
171 ****P<0.0001; n=76-103 neuromasts; N=12 trials).
172 As described in Fig. 2 F, we found on average ~half of L3-L5 neuromasts examined
173 showed “disrupted” hair-cell morphology immediately following sustained stimulus exposure. To
174 define the associations between overall neuromast morphology and specific structural changes
175 in mechanically injured neuromasts, we examined the numbers of hair cells and the percent of
176 hair cells contacted by afferent fibers in exposed neuromasts parsed into “normal” and
177 “disrupted” morphologies. With hair cell number, we observed significant loss specifically in
178 “disrupted” neuromasts, while “normal” neuromast hair-cell number appeared comparable to
179 control (Fig. 3 D; Ordinary one-way ANOVA, P=0.9995 (normal), ****P<0.0001 (disrupted)).
180 With hair-cell afferent contacts we observed a similar trend i.e., a significant number of hair cells
181 lacked afferent innervation in stimulus exposed neuromasts with “disrupted” morphology, but not

182 “normal” neuromasts (Fig. 3 E’; One sample Wilcoxon test, P>0.9999 (normal),
183 ****P<0.0001(disrupted)).

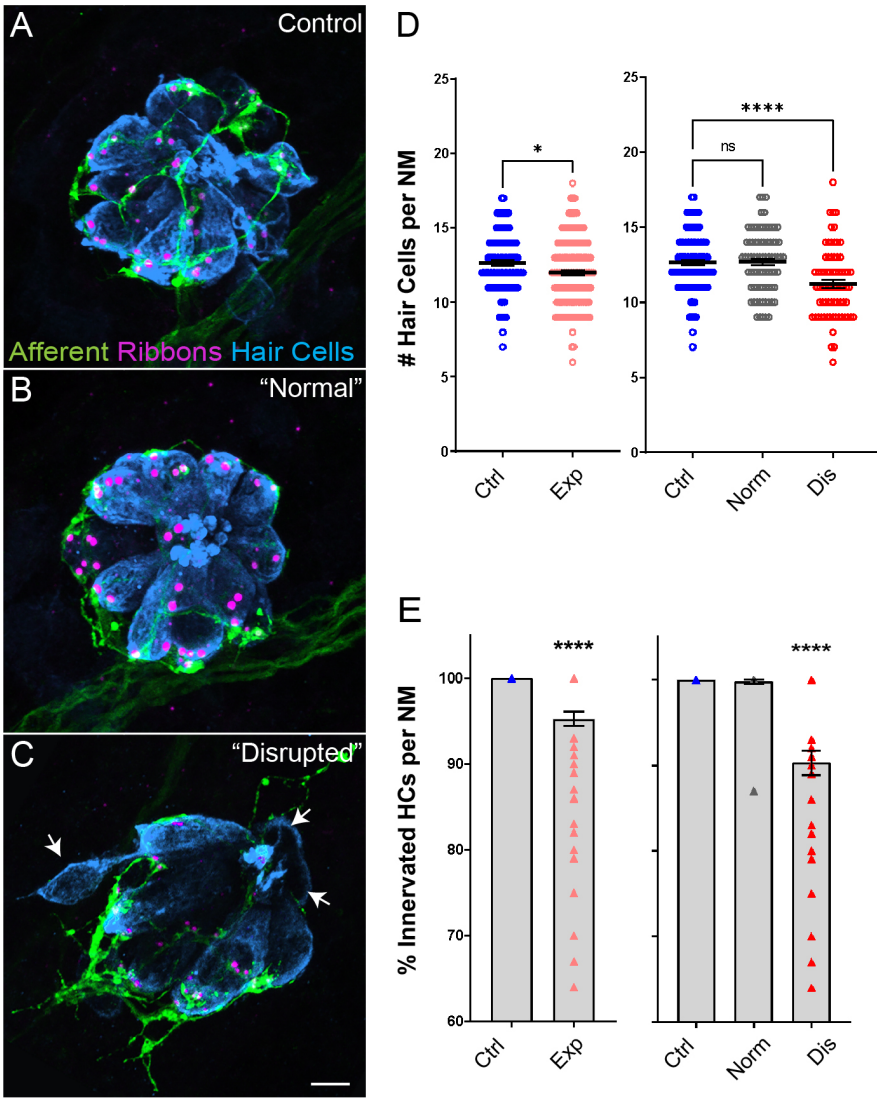

Figure 3: Hair-cell loss and de-innervation is specific to “disrupted” neuromasts.
(A-C) Representative maximum intensity projection images of control (A), or exposed lateral-line neuromasts with “normal” (B) or “disrupted” (C) morphology immediately post exposure (0 h). Synaptic ribbons (magenta; Ribeye b) and hair cells (blue; Parvalbumin) were immunolabled. Afferent neurons were expressing GFP. **(D)** Hair-cell number per neuromast (NM; L3-L5) immediately following sustained strong wave exposure. A moderate but significant reduction in hair cell number was observed (*P=0.0125) and was specific to “disrupted” neuromasts (P=0.9995 norm, ****P<0.0001 dis). Scale bar: 5μm **(E)** Percentage of neuromast hair cells innervated by afferent nerves. Each symbol represents a single neuromast; symbols in Ctrl appear as one because of overlap at 100% innervated (n=76). A significant portion of neuromast hair cells lacked afferent innervation following exposure; ****P<0.0001 sustained). Hair cells lacking afferent innervation were specifically observed in disrupted neuromast s (P>0.9999 normal, ****P<0.0001 disrupted). Pink symbols on graphs (Exp) represent pooled exposed neuromasts, while gray (Norm) and red (Dis) represent neuromasts parsed into normal and disrupted groups. Error Bars = SEM

184

185 **Mechanically overstimulated neuromasts with “normal” morphology lose a greater**
186 **number of hair-cell synapses when glutamate clearance is inhibited**

187 Hair cells contain electron-dense presynaptic specializations—called dense bodies or
188 synaptic ribbons—apposing afferent PSDs which constitute afferent synaptic contacts (Davies,
189 Tingley, Kachar, Wenthold, & Petralia, 2001; Sheets, Trapani, Mo, Obholzer, & Nicolson, 2011).
190 In the larval zebrafish lateral line, afferent nerve fibers innervate multiple hair cells per
191 neuromast forming ~3-4 synaptic contacts per hair cell. To determine whether strong water
192 current exposure contributed to hair-cell synapse loss, we counted the number of intact
193 synapses (ribbons juxtaposed to PSDs; Fig. 4 A-C) in control and exposed larvae. We observed

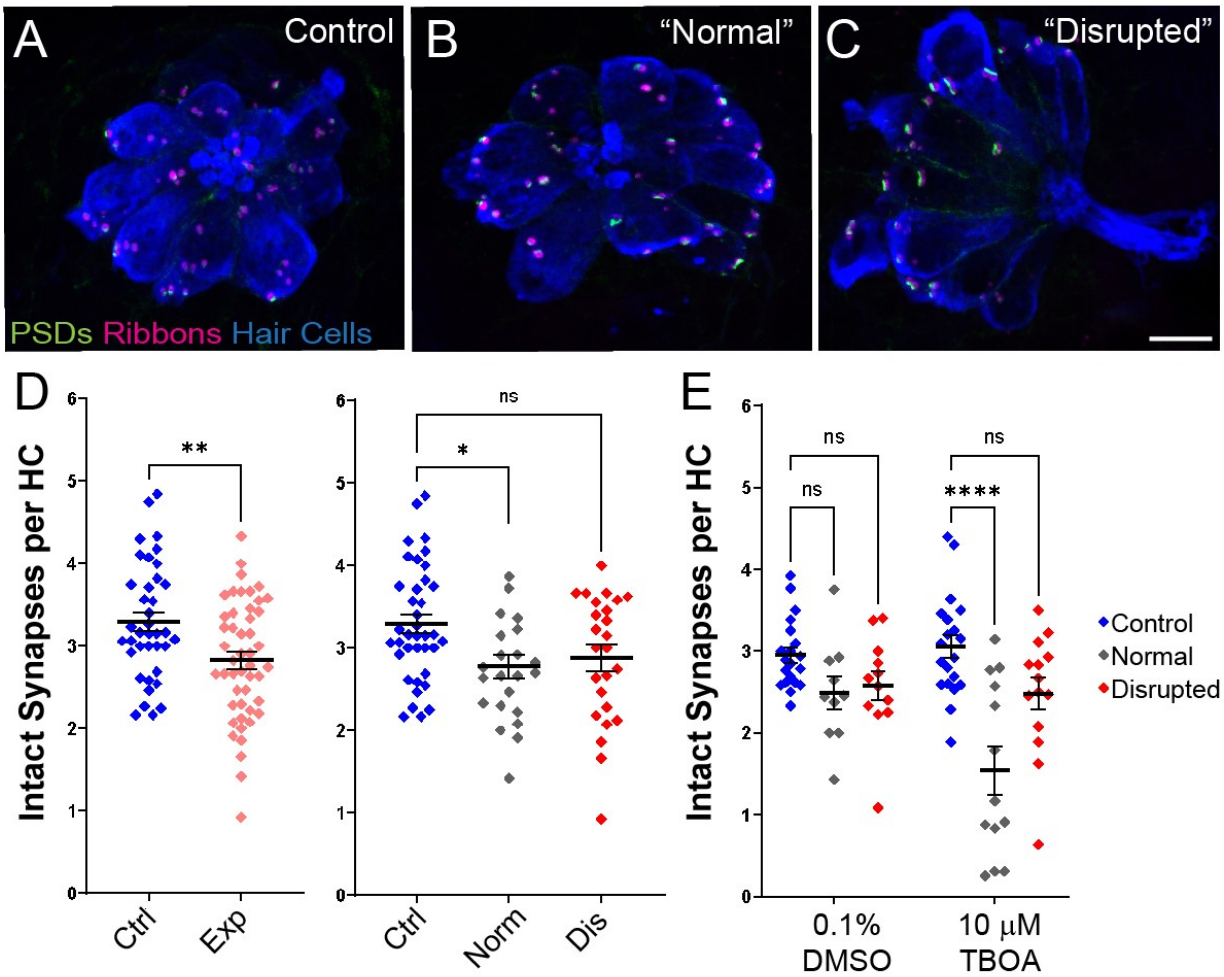

Figure 4: Synapse loss is observed in hair cells following mechanical overstimulation and exacerbated by blocking glutamate uptake. **A-C)** Representative maximum intensity projection images of unexposed (A), or wave stimulus exposed lateral-line neuromast with "normal" (B) or "disrupted" (C) morphology. Synaptic ribbons (magenta; Ribeye b), PSDs (green; MAGUK) and hair cells (blue; Parvalbumin) were immunolabled. Scale bar: 5μm **(D)** Intact synapses per neuromast hair cell. Each symbol represents an individual neuromast (L3-5). Pink symbols on graph (Exp) represent pooled exposed neuromasts, while gray (Norm) and red (Dis) represent neuromasts parsed into normal and disrupted groups. The number of intact synapses per hair cell was significantly reduced following exposure (Unpaired T-Test **P=0.0036) and was somewhat more pronounced in "normal" neuromasts than "disrupted" (One-way ANOVA, *P=0.0213 normal, P=0.0685 disrupted). **(E)** The number of intact synapses per hair cell in larvae co-treated with TBOA (to block glutamate uptake) or drug carrier alone during exposure. Synapse loss was significantly greater in "normal" NMs co-exposed to TBOA (Two-way ANOVA. ****P<0.0001). Error Bars = SEM

194 a significant reduction in the number of intact synapses per hair cell following sustained
195 exposure (Fig. 4 D; Unpaired t-test, **P=0.0036). When we compared "normal" and "disrupted"
196 neuromasts following exposure, we observed a loss of intact synapses per hair cell in all
197 exposed neuromasts, with significantly fewer synapses in "normal" exposed neuromasts relative
198 to control (Fig. 4 E; Ordinary one-way ANOVA, *P=0.0213 (normal), P=0.0685 (disrupted)).

199 Additionally, significant synapse loss was observed in the neuromasts of fish exposed to the
200 less mechanically damaging “periodic” stimulus (Supplemental Fig. 1 F’). Taken together, these
201 data revealed that synapse loss was observed in all mechanically overstimulated neuromast
202 hair cells, including neuromasts that were not mechanically disrupted.
203 Previous studies indicate that excess glutamate signaling may be a key factor driving
204 inner hair-cell synapse loss following exposure to damaging noise (Chen, Kujawa, & Sewell,
205 2010; Kim et al., 2019). We therefore inhibited glutamate clearance from neuromast hair-cell
206 synapses by pharmacologically blocking uptake with the glutamate transporter antagonist
207 Threo-beta-benzyloxyaspartate (TBOA) during sustained stimulus exposure. We observed a
208 significantly greater degree of hair-cell synapse loss in stimulated neuromasts with “normal”
209 morphology co-treated with TBOA than in stimulated neuromasts co-treated with drug carrier
210 alone (Fig. 4 E; Two-way ANOVA ****P<0.0001 “normal” TBOA), suggesting glutamate
211 excitotoxicity contributes to hair-cell synapse loss observed in mechanically overstimulated
212 neuromasts with intact morphology.
213 To further characterize synapse loss in relation to afferent neurite retraction, we
214 examined fish in which we immunolabeled synaptic ribbons, PSDs, afferent nerve fibers, and
215 hair cells (Fig. 5 A,B). We then quantified instances where synapses, i.e. juxtaposed pre- and
216 postsynaptic components associated with hair cells, were no longer adjacent to an afferent
217 nerve terminal. As these synapses appeared detached and suspended from their associated
218 neurons, making them no longer functional, we refer to them as synaptic debris. While we rarely
219 observed synaptic debris in unexposed neuromasts, we observed a greater relative frequency
220 of synaptic debris in neuromasts exposed to strong water current stimulus (Fig. 5 C; One
221 sample Wilcoxon test, P=0.1250 (control), *P=0.0313(normal), **P=0.0039(disrupted)).
222 Cumulatively, we observe two distinct types of morphological damage to afferent synapses in
223 mechanically overstimulated neuromasts: loss of synapses that is exacerbated when glutamate
224 uptake is blocked and a higher incidence of synaptic debris that appear detached from afferent
225 neurites.

226 **Mechanically overstimulated lateral line neuromasts show signs of hair-cell injury and**
227 **macrophage recruitment**

228 The inner ears of birds and mammals possess resident populations of macrophages,
229 and additional macrophages are recruited after acoustic trauma or ototoxic injury (Warchol,
230 2019). A similar macrophage response occurs at lateral line neuromasts of larval zebrafish after
231 neomycin ototoxicity (Warchol, Schrader, & Sheets, 2021). Analysis of fixed specimens, as well
232 as time-lapse imaging of living fish (e.g., Hirose, Rutherford and Warchol, 2017), has

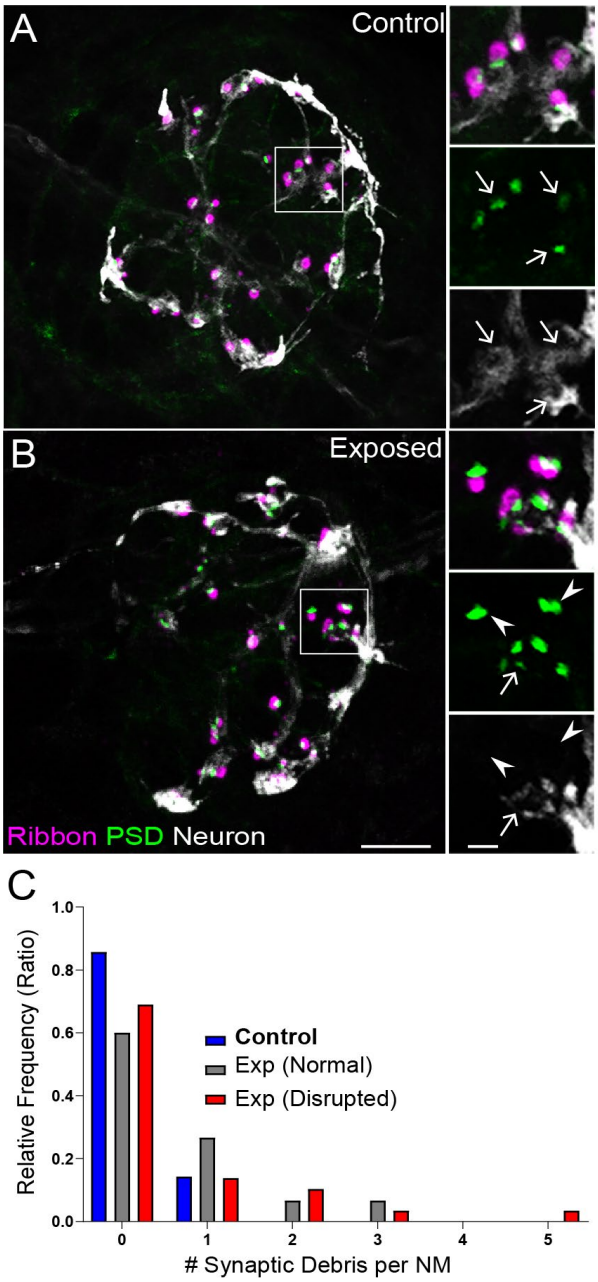

Figure 5: Mechanically overstimulated neuromasts showed retracted neurites and detached synaptic debris. **(A-B)** Representative images of control (A) and exposed (B) neuromasts. Synaptic ribbons (magenta; Ribeye b) and PSDs (green; MAGUK) were immunolabeled; hair cells were also immunolabeled, but not shown for clarity. Afferent neurons (white) were labeled with GFP. Insets: Arrows indicate intact synapses adjacent to afferent neurons; arrowheads (B) indicate synaptic debris. Scale bars: 5μm (main panels), 1μm (insets). **(C)** Frequency histogram of observed synaptic debris per neuromast (NM). While control neuromasts occasionally had 1 detached synapse, exposed neuromasts were observed that had up to 5 detached synapses.

demonstrated that macrophages migrate into neomycin-injured neuromasts and actively phagocytose the debris of dying hair cells. To determine whether a similar inflammatory response also occurs after mechanical injury to the lateral line, we characterized macrophage behavior after sustained 60 Hz stimulation. These studies employed Tg(*mpeg1:yfp*) transgenic fish, which express YFP in all macrophages and microglia. Fish were fixed immediately after exposure, or allowed to recover for 2, 4 or 8 hours. Control fish consisted of siblings that received identical treatment, but were not exposed to mechanical stimulation. Data were obtained from the two terminal neuromasts from the pLL of each fish (Fig. 6 A). in agreement

242

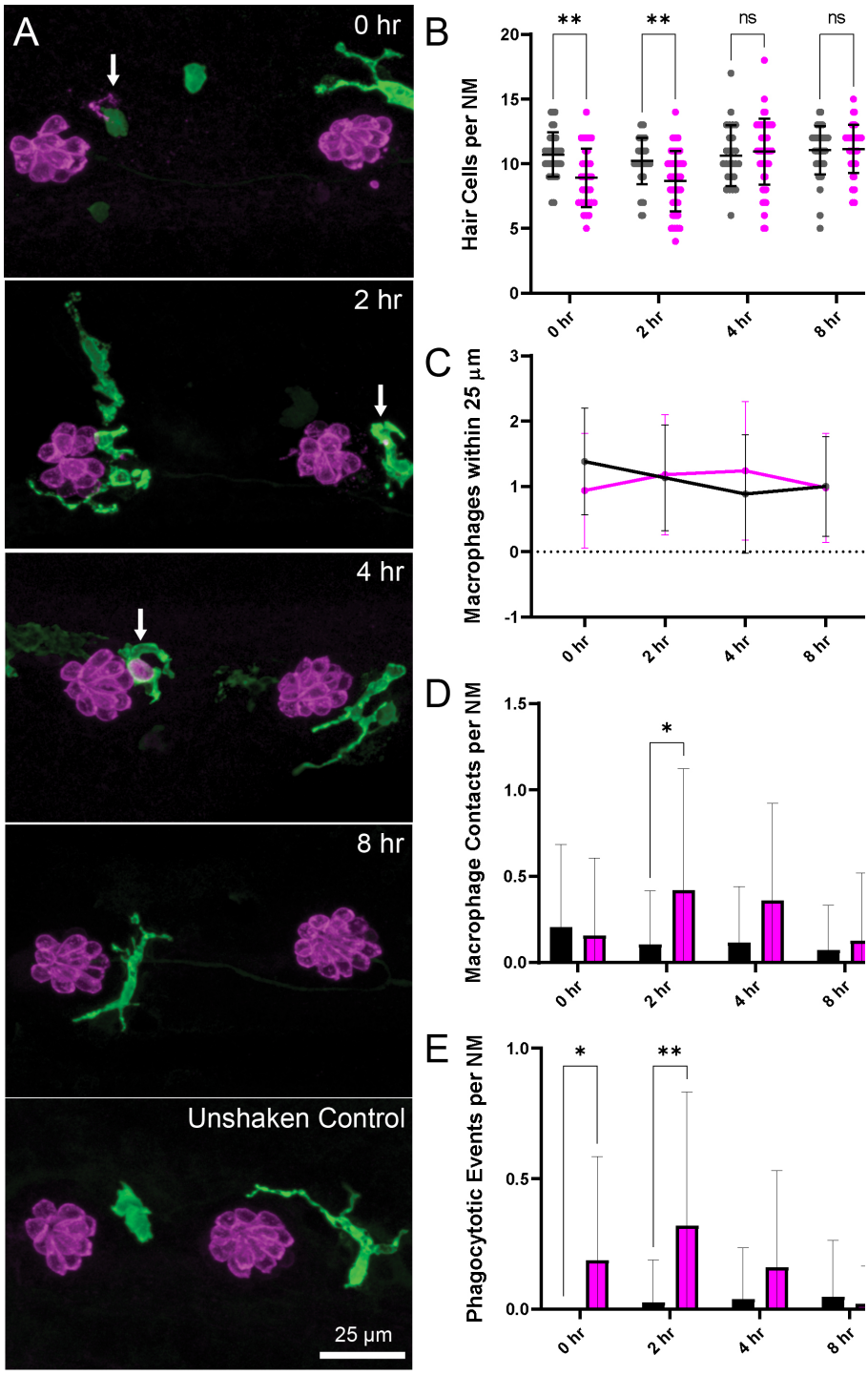

Figure 6. Macrophage response to mechanical overstimulation of lateral line hair cells. Experiments used fish that express YFP under regulation of the macrophage-specific *mpeg1* promoter. All images and data were collected from the two distal-most neuromasts of the posterior lateral line (Fig 2A; term). **(A)** Macrophages (green) responded to mechanical injury by entering neuromasts, contacting hair cells and internalizing otoferlin-labeled debris (arrows, magenta). Images show examples of macrophage behavior at different time points after noise trauma. **(B)** Quantification of hair cell number, which was significantly reduced at 0-2 hr after noise exposure (Mixed-effects analysis: **P<0.003). **(C)** Quantification of macrophages within a 25 µm radius of the terminal neuromasts at 0-8 hr after noise injury. Most neuromasts possessed 1-2 nearby macrophages and this number was not changed by noise exposure. **(D)** Quantification of direct contacts between macrophages and hair cells. Macrophage-hair cell contacts were counted at each survival time after noise exposure and normalized to the total number of sampled neuromasts. Increased levels of contact were observed at 2 and 4 hr after noise (*P=0.0243). **(E)** Quantification of phagocytosis as a function of post-noise survival time. Macrophages that had internalized otoferlin-labeled material were counted at each time point and normalized to the total number of sampled neuromasts. The percentage of macrophages that contained such debris was significantly increased at 0-2 hr after strong current (*P=0.0465; **P=0.0013). Data were obtained from 26-50 neuromasts/time point. Error Bars = SD

243 with data shown in Fig. 3 D, we observed a modest but significant decline in hair-cell number in
244 specimens that were examined immediately and at 2 hours after sustained exposure (Fig. 6 B;
245 **P<0.003). Consistent with earlier studies (Hirose, Rutherford, & Warchol, 2017), 1-2
246 macrophages were typically present within a 25 µm radius of each neuromast (Fig. 6 C). In

247 uninjured (control) fish, those macrophages remained outside the sensory region of the
248 neuromast and rarely contacted hair cells. However, at 2, 4 and 8 hours after sustained
249 stimulus, we observed increased macrophage-hair cell contacts (Fig. 6 D; *P=0.024), as well as
250 the presence of immunolabeled hair-cell debris within macrophage cytoplasm (suggestive of
251 phagocytosis, Fig. 6 A, 4 h., arrow). Macrophage-hair cell contact and phagocytosis peaked at 2
252 hours after exposure (Fig. 6 E; **P= 0.0013 (2 h)). Notably, the numbers of macrophages within
253 a 25 μm radius of each neuromast remained unchanged at all time points after exposure,
254 suggesting that the inflammatory response was mediated by local macrophages and that
255 mechanical injury did not recruit macrophages from distant locations (Fig. 6 C). This pattern of
256 injury-evoked macrophage behavior is qualitatively similar to the macrophage response
257 observed in the mouse cochlea after acoustic trauma (Hirose et al., 2005; Kaur et al., 2019;
258 Kaur et al., 2015).

259 **Mechanically injured neuromasts fully repair following exposure**

260 To determine if damage to mechanically injured neuromasts was progressive, persistent,
261 or reversible, we characterized neuromast morphology, hair-cell number, innervation, and
262 synapse number at both 2 hours and 48 hours following sustained exposure to strong current
263 stimulus. We observed a decrease in the percentage of neuromasts showing “disrupted”
264 morphology 2 hours following exposure, relative to fish fixed immediately following exposure
265 (Fig. 7 A; 54% disrupted (0 h) vs. 32% disrupted (2 h); N=4 trials), suggesting that physical
266 disruption of neuromast morphology following mechanical injury is rapidly reversible. Consistent
267 with this observation, the average hair-cell number per neuromast at 2 hours post-exposure
268 appeared to recover (Fig. 7 B; Unpaired t-test, P=0.3011; n=63-75 neuromasts; N=7 trials).
269 Recovery of hair-cell number occurred within 2-4 hours (Fig. 6 A, B) and corresponded with
270 macrophages infiltrating neuromasts and phagocytosing hair-cell debris (Fig. 6 A, E) as well as
271 a slight increase in supporting cell proliferation (Supplemental Figure 3 A,C). We also observed,
272 compared to immediately following exposure, a lesser degree of afferent fiber retraction (Fig. 7
273 C; One sample Wilcoxon test, ***P=0.0010; n=38-44 neuromasts; N=6 trials) and some synaptic
274 recovery 2 hours following mechanical injury (Fig. 7 D, Unpaired t-test, *P=0.0271; n=37-47
275 neuromasts; N=6 trials) indicating partial recovery of innervation and synapse number.

276 A recent study characterized zebrafish lateral-line hair-cell damage induced by exposure
277 to ultrasonic waves and reported a delayed hair-cell loss 48-72 hours following exposure (Uribe
278 et al., 2018). To determine if lateral line neuromasts damaged from strong water current
279 stimulus generated by our apparatus either continued to recover or underwent further delayed
280 damage, we examined hair-cell morphology, number, and innervation 48 hours following

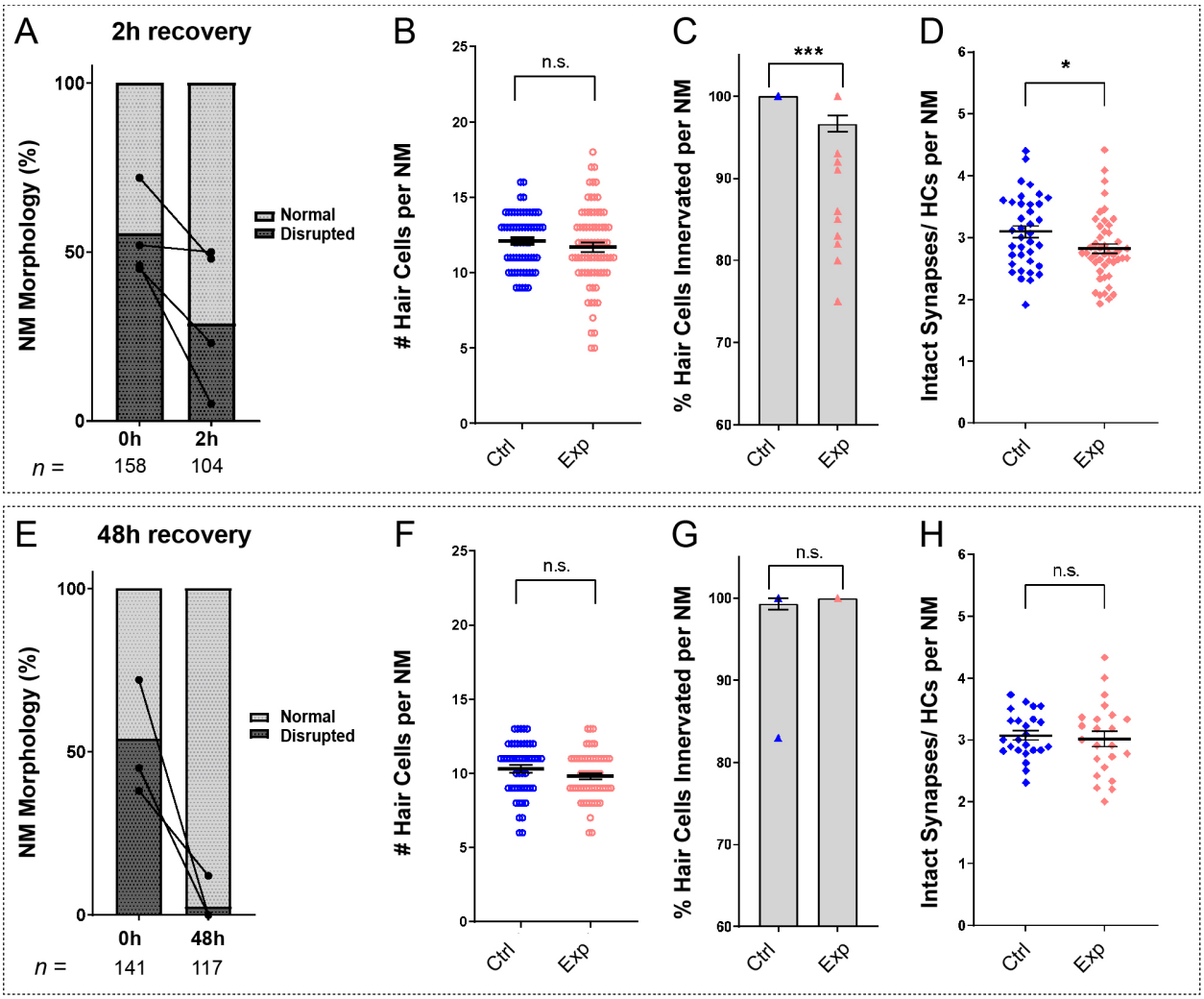

Figure 7: Mechanically overstimulated neuromasts recover hair-cell morphology, innervation, and synapse number by 48 hours following sustained exposure. **(A,E)** Average percentage of exposed neuromasts with "normal" vs. "disrupted" morphology following exposure. Each dot represents the percentage of disrupted neuromasts (L3-L5) in a single experimental trial; lines connect data points from the same cohort of exposed fish following 2 hours (A) or 48 hours (E) recovery. **(B,F)** Hair-cell number per neuromast was nearly comparable to control following 2 hour (B, P=0.3011) and 48 hour recovery (F, P=0.1253). **(C,G)** The percentage of neuromast hair cells lacking afferent innervation was still significant following 2 hour recovery (C, ***P=0.0010), but was fully recovered by 48 hours (G, P>0.9999). **(D,H)** Significantly fewer intact synapses per hair cell were observed 2 hours following exposure (D, *P=0.0271), but appeared to recover by 48 hours (H, P=0.7044). Each pink symbol on graphs (Exp) represent an individual exposed neuromast; both normal and disrupted were pooled for the analysis. Error Bars = SEM

sustained stimulus exposure. Nearly all exposed neuromasts examined showed "normal" HC morphology (Fig. 7 E) with no difference in hair-cell number (Fig. 7 F; Unpaired t-test, P=0.1253; n=49-57 neuromasts; N=5 trials). Hair-cell innervation after 48 hours was comparable to control fish (Fig. 7 G; One sample Wilcoxon test, P>0.9999; n=24-28 neuromasts; N=5 trials). We also surveyed whether synapse loss resulting from overstimulation persisted in exposed neuromasts

and observed synapse number per hair cell also appeared to fully recover (Fig. 7 H; Unpaired t-test, =0.7044; n=23-24 neuromasts; N=5 trials).

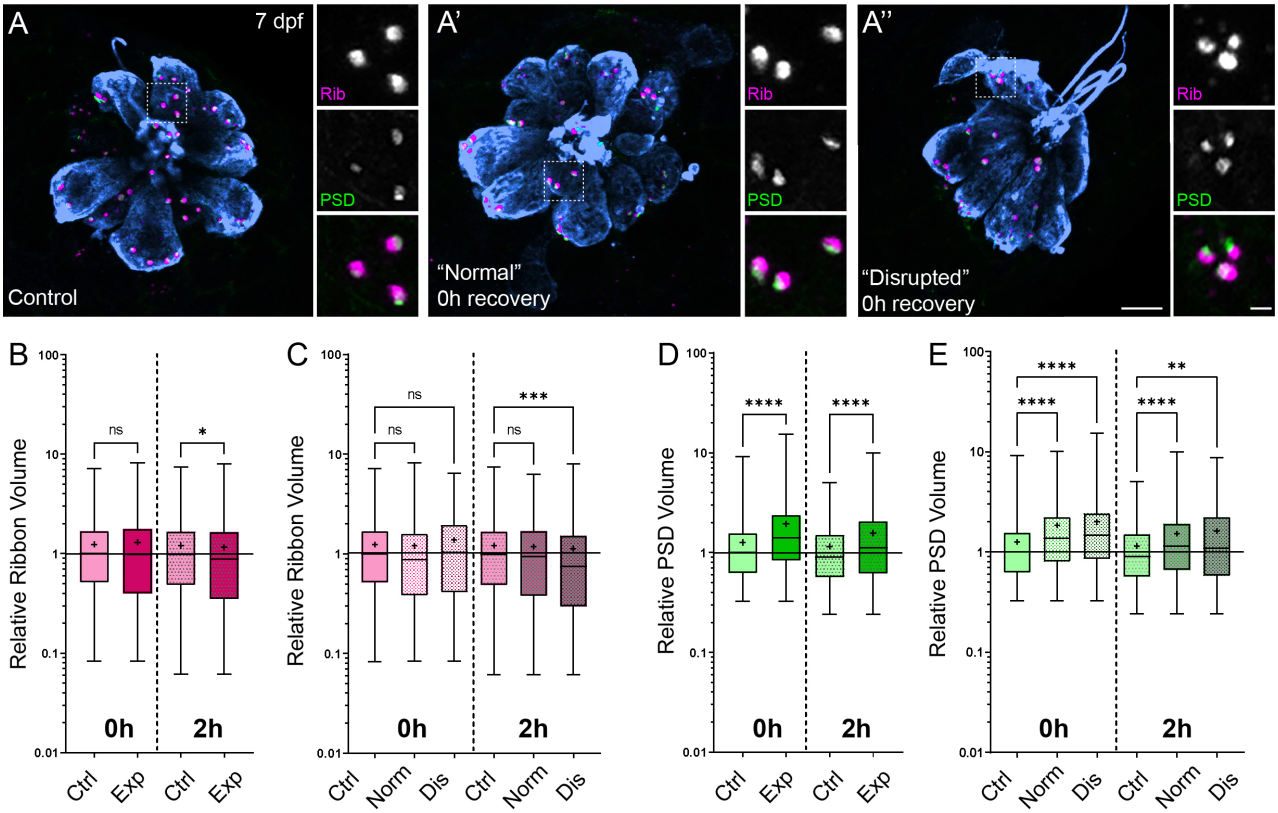

Figure 8: Changes in synaptic ribbon and PSD sizes following sustained mechanical overstimulation. **(A-A'')** Representative images of control (A) and exposed (A', A") neuromasts. Synaptic ribbons (magenta; Ribeye b), PSDs (green; MAGUK), and hair cells (blue, Parvalbumin) were immunolabeled. Scale bars: 5µm (main panels), 1µm (insets). **(B-E)** Box and whisker plots of relative synapse volumes normalized to 0h control. Whiskers indicate the min. and max. values; "+" indicates the mean value, horizontal lines indicate the relative median value of the control. (B) Ribbon volume appeared comparable to control immediately following exposure but was reduced 2 hours after exposure (*P=0.0195). (C) Significant reduction in ribbon size relative to control was specific to disrupted neuromasts (Kruskal-Wallis test: ***P=0.0004 (2h)). (D) Significantly larger PSDs were observed both immediately and 2 hours following exposure (****P<0.0001). (E) Enlarged PSDs were present in both "normal" and "disrupted" exposed neuromasts, with a greater enlargement observed 0h post-exposure (Kruskal-Wallis test: ****P<0.0001 (0h) ; ***P=0.0001, **P=0.0024 (2h)).

PSDs are enlarged in all neuromasts following mechanical overstimulation

Previous studies in mice and guinea pigs indicate moderate noise exposures modulate the size of synaptic components (Kim et al., 2019; Song et al., 2016). To determine if pre- and postsynaptic components were also affected in our model, we compared the relative volumes of neuromast hair-cell presynaptic ribbons and their corresponding PSDs in control and stimulus exposed larvae. We observed a moderate reduction in synaptic-ribbon size following exposure; ribbon volumes were significantly reduced relative to controls following 2 hours recovery (Fig. 8

295 B; Kruskal-Wallis test *P=0.0195; N=3 trials), and this reduction was specific to "disrupted"
296 neuromasts (Fig. 8 C).
297 While the changes in ribbon volume we observed were modest and delayed in onset, we
298 saw dramatic enlargement of PSDs immediately and 2 hours following exposure (Fig. 8 D;
299 Kruskal-Wallis test ****P<0.0001; N=3 trials). In contrast to the observed reduction in ribbon
300 size, relative PSD volumes were significantly enlarged in all exposed neuromasts regardless of
301 whether neuromast morphology was "normal" or "disrupted" (Fig. 8 E). These data reveal
302 enlarged PSDs as the predominant structural change in mechanically overstimulated neuromast
303 hair- cell synapses.

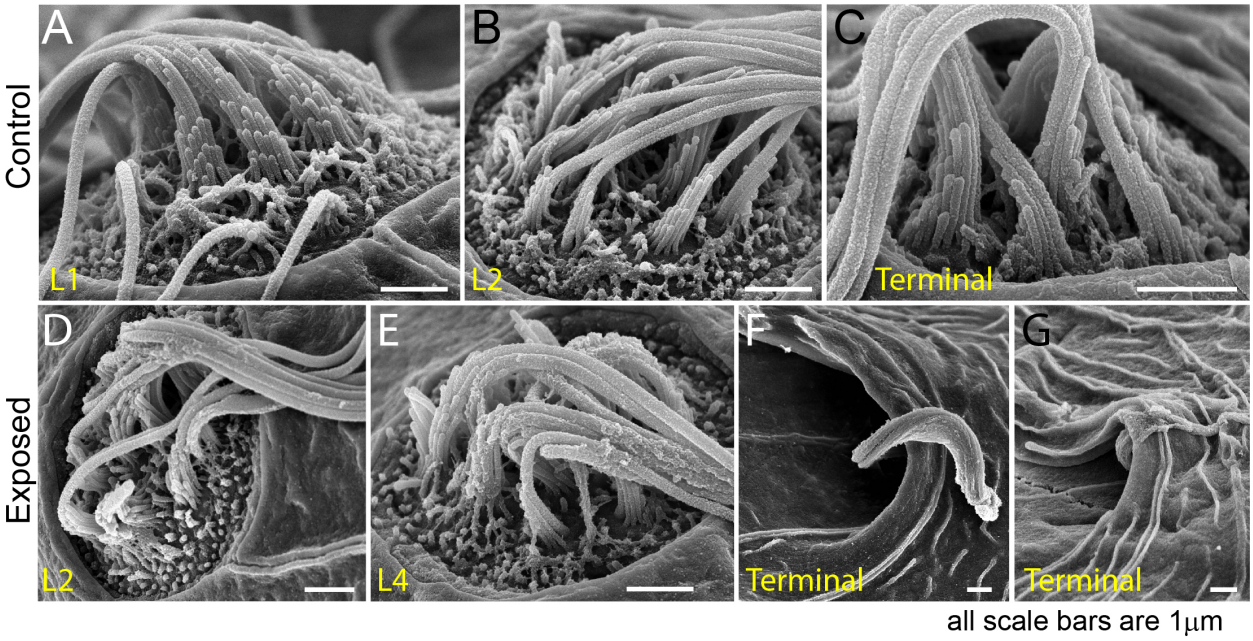

Figure 9: Scanning electron microscopy imaging of tail neuromasts following mechanical injury confirms the damage is more prominent for posterior neuromasts. **(A-C)** Representative images of tail neuromasts of control fish larvae, presented as they are positioned on the larva: L1, L2 and terminal neuromasts. Each hair cell carries a tubulin-based primary cilium (kinocilium), which is thicker than the multiple actin-filled, mechanosensitive stereocilia arranged in a staircase. **(D-G)** Examples of tail neuromasts immediately following sustained stimulus exposure, presented as they are positioned on the larva: L2, L4, and two terminal neuromasts highlighting different levels of damage, with much more pronounced damage evident on terminal neuromasts. Scale bars: 1 μm

304 **Mechanically injured neuromasts have damaged kinocilia, disrupted hair-bundle**
305 **morphology, and reduced FM1-43 uptake**
306 An additional consequence of excess noise exposure in the cochlea is damage to
307 mechanosensitive hair bundles at the apical end of hair cells and, correspondingly, disruption of
308 mechanotransduction (Wagner & Shin, 2019). Larval zebrafish lateral-line hair cells each have a
309 hair bundle consisting of a single kinocilium flanked by multiple rows of actin-rich stereocilia
310 (Kindt, Finch, & Nicolson, 2012). To determine if our exposure protocol damaged apical hair-cell

structures, we used confocal imaging and scanning electron microscopy (SEM) to assess hair bundle morphology in both unexposed control larvae and larvae fixed immediately following sustained exposure. All neuromasts throughout the fish were evaluated, but to remain consistent with our fluorescence imaging results, we closely assessed the appearance of the caudal pLL neuromasts. We found the caudal neuromasts to be more damaged than the ones positioned more rostrally: the frequency of neuromasts with apparently disrupted appearance

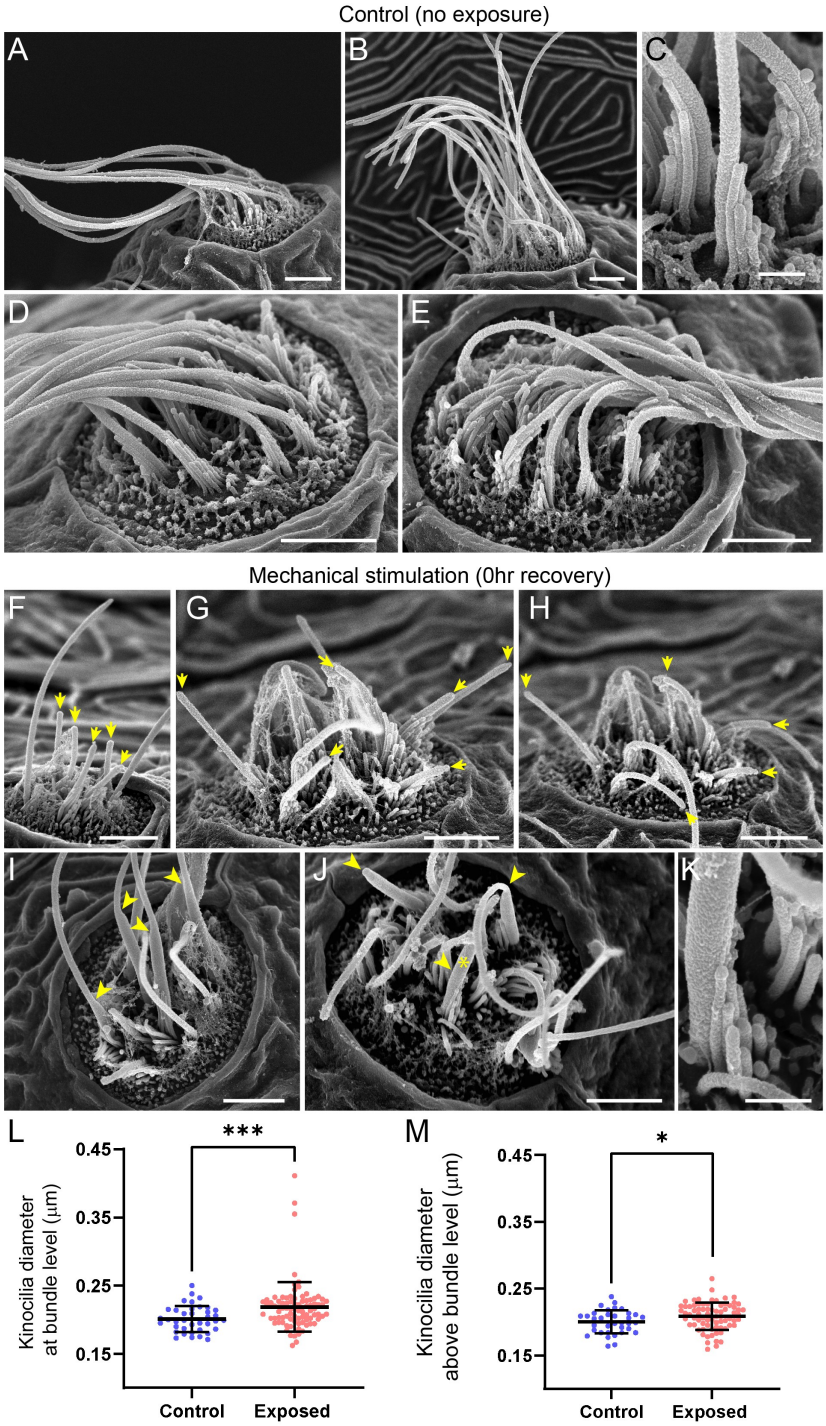

Figure 10: Scanning electron microscopy imaging of neuromasts following mechanical injury reveals disorganized hair cell stereocilia bundles and damaged kinocilia. **(A-E)** Representative images of tail neuromasts of control fish larvae. Each hair cell carries a kinocilium, which is visibly thicker than its neighboring actin-filled, mechanosensitive stereocilia: see panel C featuring both structures at higher magnification (the kinocilium diameter is 220 nm, while stereocilia measured 90-110 nm). The kinocilia of control neuromasts are long (10-15 µm) and bundled together, while the stereocilia bundles have an apparent staircase arrangement. **(F-K)** Representative images of damaged tail neuromasts immediately following noise exposure featuring short (F-H, yellow arrows), disorganized (G, H), and swollen (I-K, yellow arrowheads) kinocilia, and disorganized stereocilia. (K) Same stereocilia bundle as in J marked with an asterisk at higher magnification to highlight the difference in the diameter of the kinocilium (360 nm) and neighboring stereocilia (85-100 nm) for noise exposed hair cells, as compared to the control hair cells in C. Scale bars: A, B, D-J – 2 µm; C, K – 500 nm. **(L-M)** Kinocilia diameter at bundle level (L; Mann Whitney test ***P=0.0007) and 3-5 µm above bundle level (M; Unpaired t-test *P=0317). Exposed NM data in L were not normally distributed (D'Agostino-Pearson test ****P<0.0001). Error Bars = SD

317 increased the closer its position to the tail (Fig. 9). This is consistent with our fluorescence
318 observations (Fig. 2 F; Supplemental Fig. 4 B) in which L5 neuromasts were more likely to be
319 disrupted than more anteriorly positioned L3. In a few extreme cases, terminal neuromasts
320 appeared engulfed by the surrounding skin, with only the bundle of kinocilia visible through the
321 sleeve-like opening of the skin (Fig. 9 F,G).

322 A closer examination of neuromast morphology revealed a difference of the kinocilia
323 length and bundling. The neuromasts of the control fish carry a bundle of long (10-15 μm),
324 uniformly shaped kinocilia (Fig. 10 A-E; Supplemental Fig. 4 A). In contrast, the neuromasts of
325 the fish fixed immediately after sustained exposure often appear to carry much shorter kinocilia
326 (Fig. 10 F-H, yellow arrows), which lack bundling and, in some cases, pointing to different
327 directions (Fig. 10 G,H; Supplemental Fig. 4 B). The apparent kinocilia length difference
328 between control and overstimulated neuromasts suggests at least some kinocilia could be
329 undergoing a catastrophic damage event at the time of stimulation, as their distal parts break off
330 the hair cells. This is further supported by some examples of kinocilia with thicker, 'swollen'
331 proximal shafts closer to the cuticular plate of the cell, some of which extend into a thinner distal
332 part while others appear to lack the distal part completely (Fig. 10 I-K, yellow arrowheads).
333 Accordingly, the average diameter of kinocilia at the level of the hair bundle (L2-5) was
334 significantly larger than control, with a few kinocilia showing dramatically thicker widths ~2x
335 greater than the thickest control (Fig. 10 L; ***P=0.0007). When measured ~3-5 μm above the
336 bundle, the exposed neuromast kinocilia have a somewhat larger average diameter relative to
337 control, but not as dramatic as observed at the base (Fig. 10M; *P=0.0243). Stereocilia bundles
338 from both groups of animals carried tip links, but we were unable to systematically evaluate and
339 quantify their abundance. However, we observed signs of damaged bundle morphology
340 following overstimulation, as they often appeared splayed, with gaps between the rows of
341 stereocilia (Fig. 10 I, J) .

342 To determine the effect of mechanical overstimulation on hair-bundle function, we
343 assessed mechanotransduction by briefly exposing larvae to the mechanotransduction-channel
344 permeable dye FM1-43 (Toro et al., 2015). While most hair cells showed a dye uptake in both
345 experimental groups, we observed a significant reduction in the relative intensity of FM1-43
346 immediately following exposure (Fig. 11 A-C, G; ****P<0.0001). Reduction of FM1-43 uptake
347 appeared to correspond with the degree of mechanical displacement of neuromasts, as we
348 observed notably less relative fluorescence in "disrupted" neuromasts compared to neuromasts
349 with "normal" morphology (Fig. 11 H; ****P<0.0001 (disrupted), ***P=0.0009 (normal)).

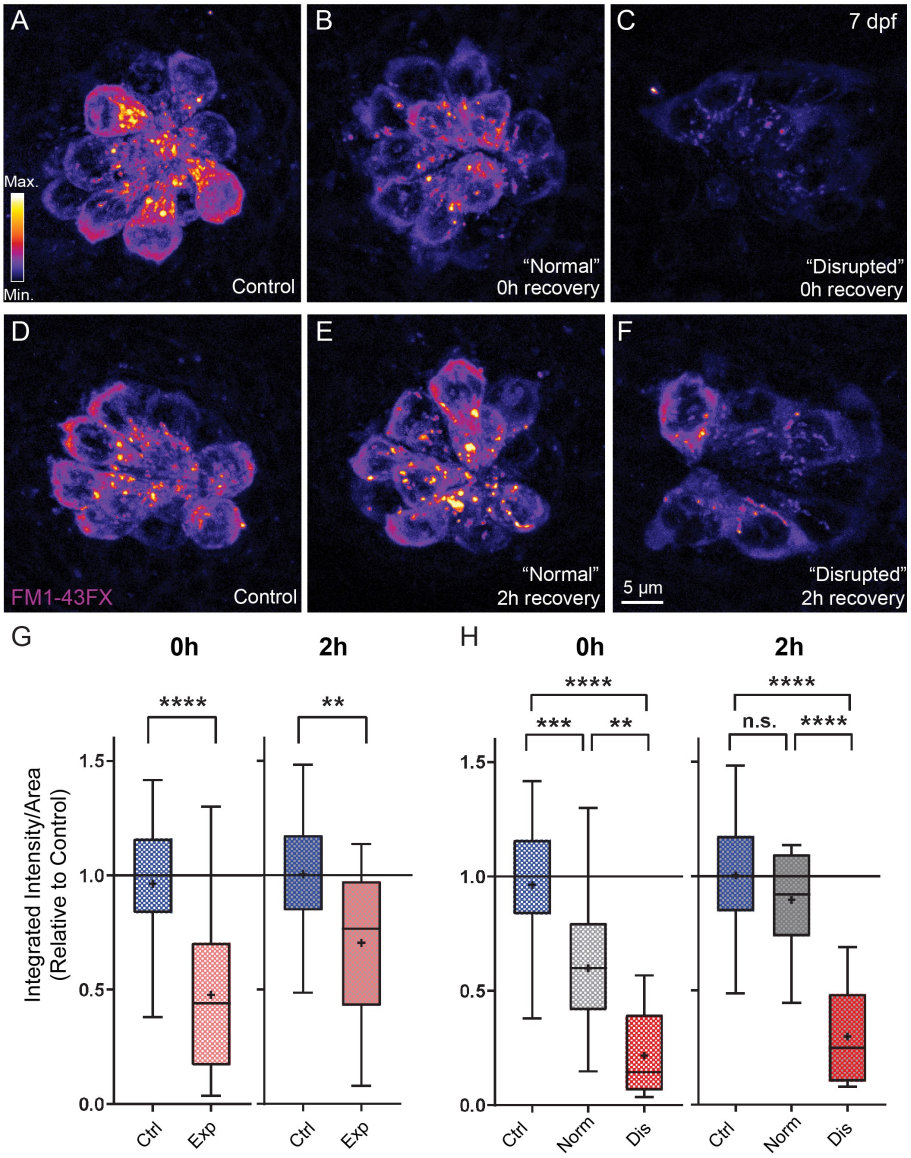

***Figure 11: Hair-cell mechanotransduction is reduced following mechanical overstimulation.* (A-F)** Representative images of FM1-43FX fluorescent intensity immediately (A-C) or 2 hours (D-F) following exposure. Note that fluorescent intensity appears visibly and dramatically reduced in "disrupted" neuromasts (C,F) and somewhat reduced in "normal" neuromasts 0h post exposure (B). **(G)** Quantified FM1-43FX fluorescence intensity measurements indicate recovery of mechanotransduction in exposed neuromasts (Unpaired t-test: ****P<0.0001 (0h), **P=0.0043 (2h)). **(H)** FM1-43FX fluorescence in "normal" exposed neuromasts is significantly reduced at 0h but appears to fully recover by 2h post-exposure. By contrast, fluorescence intensity in "disrupted" neuromasts modestly recovered 2h post-exposure. (Ordinary one-way ANOVA ****P<0.0001, ***P=0.0009, **P=0.0078 (0h) ; ****P<0.0001 (2h)).

Corresponding to what we observed with hair-cell morphology and number (Fig. 7 A,B), mechanotransduction appears to rapidly recover; 2 hours post exposure FM1-43 uptake is less reduced (Fig. 11 D-G; **P=0.0043) and nearly fully recovered in exposed neuromasts with "normal" morphology (Fig. 11 H; ****P<0.0001 (disrupted), P=0.3846 (normal)). We further observed that FM1-43 uptake after 48 h recovery was comparable to that observed in undamaged (control) fish (Fig. 12) supporting that hair-cell morphology and function fully recover.

Discussion

To model mechanical injury resulting from noise trauma in the zebrafish lateral line, we describe here a method to mechanically overstimulate neuromasts of the posterior lateral line. Using this method, we observed: i) hair-cell synapse loss and enlarged postsynaptic densities in

all stimulus exposed neuromasts, ii) morphological displacement, hair-cell loss, and afferent neurite retraction in a subset of mechanically disrupted neuromasts, iii) an inflammatory response that peaked 2-4 hours following stimulus exposure, iv) kinocilia and hair bundle damage, and v) reduced FM1-43 uptake, suggesting damage to mechanotransduction machinery. Remarkably, mechanically injured neuromasts rapidly recover following exposure; neuromast morphology, innervation, synapse number, and mechanotransduction showed partial recovery within hours and were completely recovered by 2 days post exposure.

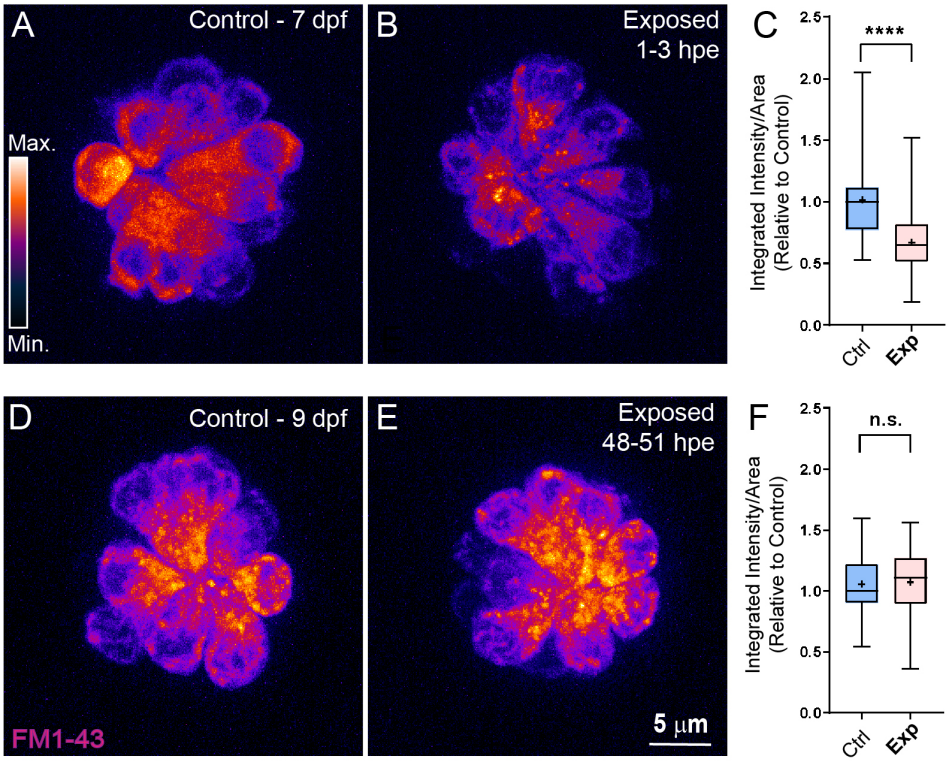

Figure 12: Hair-cell mechanotransduction fully recovers following mechanical overstimulation. Representative images of live FM1-43 fluorescent intensity 1-3 hours **(A-C)** or 48-51 hours **(D-F)** following exposure. (C) Quantified FM1-43 fluorescent intensity measurements indicate reduced mechanotransduction in exposed neuromasts (Unpaired t-test: ****P<0.0001). (F) FM1-43 fluorescence fully recovers by 48-51 hours post-exposure

Zebrafish lateral-line as a model for sub-lethal mechanical damage and noise-induced synapse loss

Mechanical damage to the zebrafish lateral line induced by strong water current stimulus is observable immediately following exposure, is specific to the lateral-line organ ,and appears to be rapidly repaired. These observations contrast with a recently published noise damage protocol for larval zebrafish which used ultrasonic transducers (40-kHz) to generate small, localized shock waves (Uribe et al., 2018). They reported delayed hair-cell death and modest synapse loss that was not apparent until 48 hours following exposure, was not accompanied by decreased mechanotransduction, and was observed in the inner ear as well as the lateral-line organs. Some of the features of the damage they observed—delayed onset apoptosis and hair-

379 cell death—may correspond to lethal damage following blast injuries. We propose features of
380 the damage we observe with our stimulus protocol—reduced mechanotransduction, hair
381 synapse loss, and rapid inflammatory response—may correspond to sub-lethal noise-induced
382 damage of hair-cell organs. Because of differences in the nature of the stimuli in these two
383 studies, it is difficult to directly compare the pathological outcomes. Mechanical overstimulation
384 in the Uribe et al., study was induced using ultrasonic (40 kHz) actuators. Such high frequencies
385 are far outside those that are detected by lateral line neuromasts (Levi et al., 2015; Trapani &
386 Nicolson, 2010) supporting that cavitation in the water medium is likely causing the observed
387 damage. In contrast, our study delivered a stimulus of high intensity 60 Hz water waves directly
388 to the fish. This frequency is within the range of sensitivity of lateral line neuromasts of larval
389 zebrafish and evoked a lateral-line mediated behavior (Fig 1B, C) suggesting that the hair cells
390 were being directly stimulated by the water motion. The present method more closely resembles
391 the techniques that are typically used to study noise damage in the mammalian cochlea, where
392 high intensity acoustic energy causes hair cell and synaptic injury in specific regions of the
393 cochlea that are best-responsive to the frequency of the stimulus. This idea is further supported
394 by the observation that synapse loss in hair cells exposed to strong current stimulation is
395 greater when glutamate uptake is blocked (Fig. 4 E), suggesting a shared mechanism of
396 glutamate excitotoxicity between noise-exposed mammalian ears and strong water current
397 stimulus exposed lateral-line organs (Kim et al., 2019; Sebe et al., 2017).

398 **Disruption of neuromast morphology is a consequence of mechanical injury**

399 Strong water current exposure produced a percentage of pLL neuromasts that were
400 morphologically “disrupted”. Several observations support that such “disrupted” neuromasts
401 represent mechanical injury to neuromast organs. One is that *lhfpl5b* mutant neuromasts, which
402 lack mechanotransduction specifically in lateral-line hair cells, were comparably vulnerable to
403 physical disruption as their wild-type siblings (Fig. 2 G;(Erickson et al., 2019)). This finding
404 supports that hair-cell activity during stimulation does not underly the physical displacement of
405 hair cells observed following strong water current stimulus. Additionally, physical disruption of
406 the neuromast affects the whole organ—hair cells and their adjacent supporting cells (Fig. 2 D).
407 This observation contrasts with what is observed in mammalian ears exposed to high intensity
408 noise, where mechanical injury to outer hair cells is localized to stereocilia disruption (H. Wang,
409 Yin, Yu, Huang, & Wang, 2011). Speculatively, displacement of hair cells in mechanically
410 injured neuromasts may be due to loss of structural support from displaced supporting cells. As
411 the lateral-line organs are superficially localized on the surface of the skin, some of the intense
412 mechanical tension applied across the tail is likely coupled to neuromasts leading to the

physical displacement of a subset of exposed neuromasts. Finally, we observed greatly reduced FM1-43 uptake in “disrupted” neuromasts and measurable changes kinocilia likely reflecting mechanical damage (Fig. 10; (Wagner & Shin, 2019)). At this time, we are unable to directly correlate the bundle or kinocilia phenotype as seen on SEM of “disrupted’ vs. “normal” neuromasts to their function as assessed by FM1-43 loading experiments. Future work on mechanical damage will focus on a close evaluation of the FM1-43 uptake and subsequent SEM imaging of the same neuromast immediately after stimulus exposure and following recovery over time.

Hair-cell overstimulation and synapse loss

We observed significant loss of hair-cell synapses in neuromasts that were exposed to strong water currents but not mechanically disrupted. Two notable observations were made in exposed neuromasts regarding synapse loss. First, loss of synapses in “normal” exposed neuromasts was markedly more severe when synaptic glutamate clearance was inhibited (Fig. 4 E), suggesting that synapse loss may reflect moderate hair-cell damage resulting from overstimulation and excess glutamate accumulation. Involvement of glutamate signaling as a key mediator of noise-induced synapse loss has recently been reported in mice; loss of glutamate signaling prevents noise-induced synapse loss and pharmacologically blocking postsynaptic Ca^{2+} permeable AMPA receptors protects against cochlear hair-cell synapse loss from moderate noise exposure (Hu et al., 2020; Kim et al., 2019). Second, synapse loss occurred in neuromasts that appeared to be fully innervated (Fig. 3 B, Fig. 4 B). This observation was somewhat more surprising given that pharmacologically activating evolutionarily conserved Ca^{2+} permeable AMPARs has been shown to drive afferent neurite retraction in the zebrafish lateral line (Sebe et al., 2017). We propose that subtle damage to afferents in “normal” exposed neuromasts may accompany synapse loss but not be apparent as neurite retraction, as single afferent processes innervate multiple hair cells of the same polarity within an individual neuromast (Dow, Jacobo, Hossain, Siletti, & Hudspeth, 2018; Faucherre, Pujol-Marti, Kawakami, & Lopez-Schier, 2009). Additionally, glutamate signaling may not be the only driver of synapse loss resulting from excess stimulation; studies in zebrafish and mice support that mitochondrial stress also contributes to hair-cell synapse loss (X. Wang et al., 2018; Wong et al., 2019). Future work using this model to examine the effect of excess mechanical stimulation on mutants with reduced glutamate release or impaired glutamate clearance (to elevate or reduce glutamate in the synaptic cleft, respectively) combined with modified mitochondrial function may define the relative roles of glutamate excitotoxicity and hair-cell mitochondrial stress to synaptic loss.

447 **Role of inflammation following mechanical injury to lateral-line organs**

448 Our results indicate that mechanical injury to neuromasts evokes an inflammatory
449 response. Prior studies of larval zebrafish have shown that macrophages reside near the
450 borders of uninjured neuromasts and migrate into neuromasts after ototoxic injury (Hirose et al.,
451 2017). We found that macrophages migrate into neuromasts within ~2 hours of mechanical
452 injury, where they contact hair cells and, in some cases, engulf hair-cell debris. Although this
453 macrophage response is similar to that which occurs after ototoxic injury to neuromasts (Carrillo
454 et al., 2016; Hirose et al., 2017; Warchol et al., 2021), the extent of hair cell loss after
455 mechanical overstimulation is much less than the injury that occurs after ototoxicity. We
456 observed macrophage entry in 30-40% of exposed neuromasts, despite modest hair cell loss
457 (Fig. 6 B,D). It is possible that the morphological changes characteristic of mechanically injured
458 neuromasts are accompanied by the release of macrophage chemoattractants. In addition,
459 studies of noise exposure to the mammalian cochlea indicate that high levels of synaptic activity
460 (without accompanying hair cell loss) can evoke macrophage migration to the synaptic region
461 (Kaur et al., 2019). In either case, the signals responsible for such recruitment remain to be
462 identified. The observation that macrophages had internalized immunolabeled hair-cell material
463 further suggests that recruited macrophages engage in the phagocytosis of hair cell debris, but
464 it is not clear whether macrophages remove entire hair cells or target specific regions of cellular
465 injury (e.g., synaptic debris; Fig. 5). In any case, our data indicate that the macrophage
466 response to mechanical injury of zebrafish lateral-line neurons is similar to that which occurs
467 after noise injury to the mammalian cochlea (Warchol, 2019) and suggests that zebrafish may
468 be an advantageous model system in which to identify the signals that recruit macrophages to
469 sites of excitotoxic injury.

470 **Hair-cell synapse morphology following mechanical overstimulation**

471 Immediately following mechanical overstimulation, the most pronounced morphological
472 change we observed in hair-cell synapses was significantly enlarged PSDs (Fig. 8 D, E).
473 Speculatively, PSD enlargement may be a consequence of reduced glutamate release from hair
474 cells following sustained intense stimulation. Mice and zebrafish fish lacking hair-cell
475 glutamatergic transmission have enlarged postsynaptic structures (Kim et al., 2019; Sheets,
476 Kindt, & Nicolson, 2012), indicating that glutamate may regulate postsynaptic size. While our
477 data do not directly support this idea, we speculate that reduced glutamatergic transmission in
478 mechanically overstimulated neuromasts may be a consequence of damaged hair bundles and
479 impaired mechanotransduction (Zhang et al., 2018). Alternatively, cholinergic efferent feedback,
480 which has been shown to hyperpolarize lateral-line hair cells, may reduce hair-cell excitability

481 during sustained strong current exposure to protect against excess glutamate release,
482 excitotoxic damage, and synapse loss (Carpaneto Freixas et al., 2021). Interestingly,
483 presynaptic ribbons were not similarly enlarged, but instead showed a modest reduction in size
484 following mechanical injury. Functional imaging of zebrafish lateral line has shown that a subset
485 of hair cells in each neuromast are synaptically silent, and these silent hair cells can become
486 active following damage (Zhang et al., 2018). As ribbon size has been observed to correspond
487 with synaptic activity (Merchan-Perez & Liberman, 1996; Sheets et al., 2012), reduction in
488 ribbon size may reflect recruitment of synaptically silent hair cells following mechanically-
489 induced damage. Future functional studies are needed to determine if mechanical
490 overstimulation recruits more active hair-cell synapses, and to verify whether glutamate release
491 from active synapses is reduced following mechanical overstimulation.

492 **Lateral-line neuromasts fully recover following mechanical damage**

493 Previous studies indicate mammalian cochlear hair cells have some capacity for repair
494 following sub-lethal mechanical damage, including tip-link repair and regeneration of a subset of
495 ribbons synapses (Indzhykulian et al., 2013; Jia, Yang, Guo, & He, 2009; Kim et al., 2019). But
496 such ability is limited, and our understanding of hair-cell repair mechanisms is incomplete. In
497 some mammalian models, synaptic ribbon repair in the cochlea following noise trauma has
498 been reported as partial but permanent, i.e. a subset of synapses are lost and do not recover. In
499 contrast, we observe complete recovery of hair cell-afferent synapses following mechanical
500 trauma to the zebrafish lateral line. The cellular mechanisms responsible for such repair are not
501 fully defined, but may involve regulation of neurite growth, glutamate signaling, inflammation,
502 and/or neurotrophic factors (Kaur et al., 2019; Kim et al., 2019; Wan, Gomez-Casati, Gigliello,
503 Liberman, & Corfas, 2014). Further study using this zebrafish model of mechanical
504 overstimulation may provide insights that will assist in the development of methods for
505 promoting complete synapse repair following damaging stimuli to the mammalian cochlea.

506 In addition to hair bundle damage and loss of synapses in morphologically intact
507 neuromasts, we also found that mechanical trauma resulted in a small degree of hair-cell loss in
508 disrupted neuromasts (Fig. 3D), but that hair-cell numbers had recovered after 2 hours (Fig. 7).
509 The mechanism that mediates this recovery is not clear. Hair-cell regeneration in the inner ear
510 can occur via direct phenotypic conversion of a supporting cell into a replacement hair cell (e.g.,
511 Warchol, 2011), and it is conceivable that such transdifferentiation could occur within 2 hours of
512 injury to recover lost hair cells. While the short recovery time is not consistent with the longer
513 process of renewed proliferation and hair-cell differentiation that underlies most hair-cell
514 regeneration in zebrafish and birds (Harris et al., 2003; Ma, Rubel, & Raible, 2008; Romero-

515 Carvajal et al., 2015), these studies were focused on recovery following profound damage and
516 complete hair-cells loss. It is also notable that hair cell synapse number fully recovers in the
517 lateral line following mechanical injury. The recovery we observe may reflect the rapid recovery
518 from mild to moderate neuromast damage that occurs in this externally localized sensory organ
519 that is directly exposed to the fish's environment and therefore continuously vulnerable to injury.
520 In summary, our data show that exposure of zebrafish lateral-line organs to strong water
521 current results in mechanical injury and loss of afferent synapses, but that these injuries recover
522 within 48 hr. Our next steps will be to define the time course for morphological and functional
523 recovery, and to determine how lateral-line mediated behavior is affected by mechanically
524 induced damage. Sub-lethal overstimulation of hair cells in the zebrafish lateral line provides a
525 useful model for defining mechanisms of damage and inflammation and for identifying pathways
526 that promote hair-cell repair following mechanically-induced injury.
527
528 Declaration of interests:
529 The authors declare no competing financial or non-financial interests.
530
531 Acknowledgments: This work was supported by the National Institute on Deafness and Other
532 Communication Disorders R01DC016066 (L.S.), R01DC017166 (A.A.I), and R01DC006283
533 (M.E.W.), Washington University Dept. of Otolaryngology (L.S.), and the Amelia Peabody
534 Charitable Fund (L.S.). We would like to thank Valentin Militchin (WashU) and Evan Foss (Mass
535 Eye and Ear) for engineering support and Mark Rutherford for thoughtful feedback on the
536 manuscript.
537

538 Method Details

539 ***Ethics Statement***

540 This study was performed with the approval of the Institutional Animal Care and Use
541 Committee of Washington University School of Medicine in St. Louis and in accordance with
542 NIH guidelines for use of zebrafish.

543 ***Zebrafish***

544 All zebrafish experiments and procedures were performed in accordance with the
545 Washington University Institutional Animal Use and Care Committee. Adult zebrafish were
546 raised under standard conditions at 27-29°C in the Washington University Zebrafish Facility.
547 Embryos were raised in incubators at 29°C in E3 media (5 mM NaCl, 0.17 mM KCl, 0.33 mM
548 $CaCl_2$, 0.33 mM $MgCl_2$; (Nüsslein-Volhard & Dahm, 2002)) with a 14 h:10 h light:dark cycle. After
549 4 dpf, larvae were raised in 100-200 ml E3 media in 250-ml plastic beakers and fed rotifers
550 daily. Sex of the animal was not considered in our studies because sex cannot be predicted or
551 determined in larval zebrafish.

552 The transgenic lines *TgBAC(neurod1:EGFP)* (Obholzer et al., 2008),
553 *Tg(tnks1bp1:EGFP)* (Behra et al., 2012), *Tg(-6myo6b:βactin-EGFP)* (Kindt et al., 2012) and
554 *Tg(mpeg1:YFP)* (Roca & Ramakrishnan, 2013) were used in this study. Fluorescent larvae were
555 identified at 3 dpf without anesthesia in E3 media. The mutant line *lhfpl5b*$^{vo35/vo35}$ was also used
556 (Erickson et al 2020).

557 ***Genotyping***

558 To genotype *lhfpl5b*$^{vo35/vo35}$ larvae and siblings after mechanical stimulation and
559 immunohistochemical labeling, ~1 mm tail tissue was excised, and genomic DNA was extracted
560 by incubation in a lysis buffer (10 mM Tris pH 8.0, 50 mM KCl, 0.3% NP-40, 0.3% Tween-20). A
561 genomic region of *lhfpl5b* was amplified by PCR using forward primer
562 GCGTCATGTGGGCAGTTTTC and reverse primer TAGACACTAGCGGCGTTGC. The
563 *lhfpl5b*^{vo35} mutation disrupts a MluCI restriction site (AATT), so PCR products were digested with
564 MluCI, and homo- and heterozygotes were resolved by differences in band size on a 1-1.5%
565 agarose gel.

566 ***Experimental Apparatus***

567 Multi-well plates containing larvae were clamped to a custom magnesium head
568 expander (Vibration & Shock Technologies, Woburn, MA) on a vertically-oriented Brüel+Kjær
569 LDS Vibrator, V408 (Brüel and Kjær, Naerum, Denmark). An additional metal plate was fitted to
570 the bottom of the multi-well dish to fill a small gap between the bottoms of the wells and the

571 head expander to eliminate flexing of the well plate relative to the head expander. Vibrometry of
572 the well bottoms and the head expander with a laser-Dopper vibrometer (OFV-2600 and OFV-
573 501, Polytec, Irvine, CA) confirmed that the well plate and head expander motion were equal at
574 stimulus frequencies. This experimental apparatus was housed in a custom sound-attenuation
575 chamber. An Optiplex 3020 Mini Tower (Dell) with a NI PCIe-6321, X Series Multifunction DAQ
576 (National Instruments) running a custom stimulus generation program (modified version of
577 Cochlear Function Test Suite) was used to relay the stimulus signal to a Brüel+Kjær LDS
578 PA100E Amplifier that drove a controlled 60 Hz vibratory stimulus along the larvae's
579 dorsoventral axis (vertically). Two accelerometers (BU-21771, Knowles, Itasca, IL) were
580 mounted to the head expander to monitor the vertical displacement of the plate. The output of
581 the accelerometers was relayed through a custom accelerometer amplifier (EPL Engineering
582 Core). A block diagram for the EPL Lateral Line Stimulator can be found here:
583 https://www.masseyeandear.org/research/otolaryngology/eaton-peabody-
584 laboratories/engineering-core).

585 ***Mechanical overstimulation of lateral-line organs in free swimming larvae***

586 At 7 dpf, free-swimming zebrafish larvae were placed in untreated 6-well plates
587 (Corning, Cat# 3736; well diameter: 34.8 mm; total well volume: 16.8 ml) with 6 ml E3 per well,
588 pre-warmed to 29°C. Up to 15 larvae were placed in each well. Individual wells were sealed with
589 Glad® Press 'n Seal plastic food wrap prior to placing the lid on the plate. An additional metal
590 plate was fitted to the bottom of the multi-well dish to fill a small gap between the bottoms of the
591 wells and the head expander.

592 Mechanical water displacement exposures (stimulus parameters: 60 Hz, 40.3 ± 0.5 m/s^2)
593 were conducted at room temperature (22-24°C) up to 2 hours after dawn. The frequency
594 selected for mechanical overexposure of lateral-line organs was based on previous studies
595 showing 60 Hz to be within the optimal upper frequency range of mechanical sensitivity of
596 superficial posterior lateral-line neuromasts (Weeg and Bass 2002, Trapani et al, 2009, Levi et
597 al, 2015). To confirm that 60 Hz was the optimal frequency to induce damage, we tested 45, 60,
598 and 75 Hz at comparable intensities. We observed at 75 Hz no apparent damage to lateral line
599 neuromasts while 45 Hz at a comparable intensity proved toxic i.e. it was lethal to the fish.

600 Exposures consisted of 20 minutes of stimulation followed by a 10-minute break and 2
601 hours of uninterrupted stimulation. We also tested periodic exposures that consisted of a series
602 of short pulses spanning 2 hours total: 2 20-minute exposures each followed by 10 minutes of
603 rest, followed by 30 minutes of stimulation, a 10-minute break, and a final 20 minutes of
604 stimulation. During the entire duration of exposure, unexposed control fish were kept in the

605 same conditions as exposed fish i.e. placed in a multi-well dish and maintained in the same
606 room as the exposure chamber. For experiments pharmacologically blocking glutamate uptake,
607 fish were co-exposed to 10 μM DL-TBOA (Tocris; Cat. No.1223) + 0.1% DMSO or 0.1% DMSO
608 alone. After exposure, larvae were either immediately fixed for histology, prepared for live
609 imaging, or allowed to recover for up to 2 days in an incubator at 29°C.

610 ***Ablation of lateral-line organ with $CuSO_4$***

611 Free-swimming larvae were exposed to freshly made 3 μM $CuSO_4$ solution in E3 for 1
612 hour, then rinsed and allowed to recover for 2 hours to ensure complete ablation of the lateral-
613 line neuromasts. Neuromast ablation was confirmed by immunofluorescent labeling of hair cells.
614 The effects of low-dose copper exposure are likely specific to lateral-line organs; a previous
615 study in zebrafish determined exposure to low-dose $CuSO_4$ for 1 hour did not alter the acoustic
616 escape response, which is similar to the fast start response we observed but evoked by higher
617 frequency stimulation (100-500 Hz) of the anterior macula of inner ear (Buck, Winter, Redfern, &
618 Whitfield, 2012).

619 ***Fast-start escape response behavior assay***

620 Images of larval swimming behavior (1000 frames per second) were acquired with an
621 Edgertronic SC1 high-speed camera (Sanstreak Corp). Image acquisition began 10 seconds
622 following stimulus onset. All subsequent analysis was performed using ImageJ. To track
623 swimming behavior, images were initially stabilized using the Image Stabilizer Plugin. In
624 stabilized images, the position of individual larval heads (located via the pigmented eyes) in
625 each frame were tracked using the Manual Tracking Plugin. Larvae were tracked over 10
626 seconds (10,000 frames total) per trial. 'Fast start' responses—defined as a c-bend of the body
627 occurring within 15 ms followed by a counter-bend— were identified manually.

628 ***Whole-mount immunohistochemistry***

629 For visualization of zebrafish lateral-line hair cells, neurons, and synapses: 7-9 dpf
630 larvae were briefly sedated on ice, transferred to fixative (4% paraformaldehyde, 1% sucrose,
631 37.5 μM $CaCl_2$, 0.1 M phosphate buffer) in a flat-bottomed 2 ml Eppedorf tubes, and fixed for 5
632 hours at 4-8°C. Fixed larvae were permeabilized in ice-cold acetone for 5 minutes, then blocked
633 in phosphate-buffered saline (PBS) with 2% goat serum, 1% bovine serum albumin (BSA), and
634 1% DMSO for 2-4 hours at room temperature (RT; 22-24 °C). Larvae were incubated with
635 primary antibodies diluted in PBS with 1% BSA and 1% DMSO overnight at 4-8°C, followed by
636 several rinses in PBS/BSA/DMSO and incubation in diluted secondary antibodies conjugated to
637 Pacific Blue (1:400), Alexa Fluor 488 (1:1000), Alexa Fluor 555 (1:1000), Alexa Fluor 647
638 (1:1000; Invitrogen), or DyLight 549 (1:1000; Thermo-Fisher) for 2 hours at RT. In some

639 experiments, fixed larvae were stained with 2.5 ug/ml 4′,6-diamidino-2-phenylindole (DAPI;
640 Invitrogen) diluted in PBS to label all cell nuclei. Larvae were mounted on glass slides with
641 elvanol (13% w/v polyvinyl alcohol, 33% w/v glycerol, 1% w/v DABCO (1,4 diazobicylo[2,2,2]
642 octane) in 0.2 M Tris, pH 8.5) and #1.5 cover slips.
643 For visualization of inflammation and macrophage recruitment: 7 dpf larvae were
644 sedated on ice, transferred to 4% paraformaldehyde fixative in PBS, then fixed overnight at 4-
645 8°C. The next day larvae were rinsed in PBS and blocked in PBS with 5% normal horse serum
646 (NHS), 1% DMSO, and 1% Triton x-100 for 2 hours at RT. Larvae were incubated with primary
647 antibodies diluted in PBS with 5% NHS and 1% Triton-x 100 overnight at RT, rinsed several
648 times in PBS, then incubated in diluted secondary antibodies listed above for 2 hours at RT.
649 Larvae were mounted on glass slides with glycerol/PBS (9:1); coverslips were sealed with clear
650 nail polish.

651 ***Primary antibodies***

652 The following commercial antibodies were used in this study: GFP (1:500; Aves Labs,
653 Inc; Cat# GFP-1020), Parvalbumin (1:2000; Thermo Fisher; Cat# PA1-933), Parvalbumin
654 (1:2000; Abcam; Cat# ab11427), Parvalbumin (1:500; Sigma-Aldrich; Cat# P3088), MAGUK
655 (K28/86; 1:500; NeuroMab, UC Davis; Cat# 75-029), Otoferlin (1:500; Developmental Studies
656 Hybridoma Bank/ HCS-1). Custom affinity-purified antibody generated against *Danio rerio*
657 Ribeye b (mouse IgG2a; 1:2000; (Sheets et al., 2011)) was also used.

658 ***Live hair-cell labeling***

659 To selectively label hair-cell nuclei, live zebrafish larvae were incubated with DAPI
660 diluted 1:2000 in E3 media for 4 minutes. Larvae were briefly rinsed 3 times in fresh E3 media,
661 then immediately exposed to mechanical overstimulation or drug. To label with FM1-43 vital dye
662 (n-(3-triethylammoniumpropyl)-4-(4-(dibutylamino)-styryl) pyridinium dibromide; ThermoFisher)),
663 free-swimming larvae were exposed to FM 1-43 at 3 μM for 20 seconds, then rinsed 3 times in
664 fresh E3 as previously described (Toro et al., 2015).
665 Live imaging of FM1-43 did not provide the temporal resolution needed to compare
666 relative uptake immediately and 2 hours following exposure. We therefore examined FM1-43
667 uptake using the fixable analogue. Free-swimming larvae were exposed to FM 1-43FX at 3 μM
668 for 20 seconds, then rinsed 3 times in fresh E3 and immediately fixed (4% paraformaldehyde,
669 4% sucrose, 150 μM $CaCl_2$, 0.1 M phosphate buffer). Relative labeling of hair cells at 1-3 hours
670 appeared comparable between live FM1-43 and FM 1-43FX. We also verified loss of FM 1-
671 43FX uptake in larvae following brief treatment with 5 mM BAPTA to disrupt tip links (Kindt et

672 al., 2012). FM 1-43 and FM 1-43FX mean signal intensity from maximum projection images was
673 calculated using ImageJ as the integrated pixel intensity divided by the area of the neuromast
674 region of interest.

675 ***EdU labeling and quantification***

676 To label proliferating cells, we used the Click-iT EdU Cell Proliferation Kit for Imaging,
677 Alexa Fluor 555 dye (Invitrogen). Following mechanical overstimulation, larvae were incubated
678 in 500 μM EdU with 0.5% DMSO in E3 for 4 hours at 28°C then fixed in 4% paraformaldehyde
679 in PBS overnight at 4°C. Larvae were washed in 3% bovine serum albumin in PBS then
680 permeabilized with 0.5% Triton-X in PBS. GFP signal in Tg[tnks1bp1:GFP] fish was amplified
681 using anti-GFP primary antibody (Aves), followed by a secondary antibody conjugated to Alexa
682 Fluor 488. The EdU detection reaction was performed according to manufacturer guidelines;
683 larvae were incubated in a reaction cocktail (4 mM CuSO4 and Alexa Fluor 555 azide in 1X
684 Click-iT reaction buffer with reaction buffer additive) for 1 hour at 25°C. Larvae were washed,
685 counterstained with Hoechst 33342, and mounted on slides with elvanol. Confocal images of
686 neuromasts were acquired using an LSM 700 laser scanning confocal microscope with a 63x
687 1.4 NA Plan-Apochromat oil-immersion objective (Carl Zeiss). The numbers of EdU+ cells per
688 neuromast were quantified in ImageJ.

689 ***Confocal imaging (fixed specimens)***

690 Images of fixed samples were acquired using an LSM 700 laser scanning confocal
691 microscope with a 63x 1.4 NA Plan-Apochromat oil-immersion objective (Carl Zeiss). Confocal
692 stacks were collected with a z step of 0.3 μm over 7-10 μm with pixel size of 100 nm (x-y image
693 size 51 x 51 μm). Acquisition parameters were established using the brightest control specimen
694 such that just a few pixels reached saturation in order to achieve the greatest dynamic range in
695 our experiments. These parameters including gain, laser power, scan speed, dwell time,
696 resolution, and zoom, were kept consistent between comparisons.

697 ***Confocal imaging (live)***

698 Live zebrafish larvae were anesthetized with 0.01% tricaine in E3, then mounted lateral-
699 side up on a thin layer of 1.5-2% low-melt agarose in a tissue culture dish with a cover-glass
700 bottom (World Precision Instruments) and covered in E3 media. Z-stack images with a z step of
701 0.5 μm were acquired via an ORCA-Flash 4.0 V3 camera (Hamamatsu) using a Leica DM6
702 Fixed Stage microscope with an X-Light V2TP spinning disc confocal (60 micron pinholes) and
703 a 63x/0.9 N.A. water immersion objective. Z- acquisition parameters w/ X-light spinning disc:

704 488 laser “20% power”, 150 ms per frame. Image acquisition as controlled by MetaMorph
705 software.

706 ***Confocal image processing and analysis***

707 All analysis was performed on blinded images. Digital images were processed using
708 ImageJ software (Schneider, Rasband, & Eliceiri, 2012). In order to quantitatively measure sizes
709 and fluorescent intensities of puncta, raw images containing single immunolabel were
710 subtracted for background using a 20-pixel rolling ball radius and whole neuromasts were
711 delineated from Parvalbumin-labeled hair cells using the freehand selection and “synchronize
712 windows” tools. Puncta were defined as regions of immunolabel with pixel intensity above a
713 determined threshold: threshold for Ribeye label was calculated using the Isodata algorithm
714 (Ridler, 1978) on maximum-intensity projections, threshold for MAGUK label was calculated as
715 the product of 7 times the average pixel intensity of the whole neuromast region in a maximum-
716 intensity projection. Particle volume and intensity were measured using the 3D object counter
717 (Bolte & Cordelieres, 2006) using a lower threshold and a minimum size of 10 voxels. To
718 normalize for differences in staining intensity across experimental trials, all volumes were
719 divided by the median control volume in each trial for each individual channel. The number of
720 particles above lower threshold was quantified using the ImageJ Maximum Finder plugin with a
721 noise tolerance of 10 on maximum-intensity projections. Intact synapses were manually counted
722 and defined as adjoining or overlapping maxima of Ribeye and MAGUK labels. The number of
723 synapses per hair cell was approximated by dividing the number of intact synapses within an
724 neuromast by the number of hair cells in the neuromast.

725 Quantitative data on macrophage response to mechanical injury were collected from the
726 two caudal-most (‘terminal’) neuromasts. Confocal image stacks were obtained using a Zeiss
727 LSM700 microscope and visualized using Volocity software. These image stacks were used to
728 derive three metrics from each neuromast. First, the number of macrophages within 25 μm of a
729 particular neuromast was determined by inscribing a circle of 25 μm radius, centered on the
730 neuromast, and counting the number of macrophages that were either fully or partially enclosed
731 by this circle. Next, the number of macrophages contacting a neuromast was determined by
732 scrolling through the x-y planes of each image stack (1 μm interval between x-y planes, 15 μm
733 total depth) and the counting macrophages that were in direct contact with Otoferlin-labeled hair
734 cells. Finally, the number of macrophages that had internalized Otoferlin-labeled material (hair-
735 cell debris) were counted and were assumed to reflect the number of phagocytic events. For
736 each metric, the recorded number reflected the activity of a single macrophage, i.e., a

737 macrophage that made contacts with multiple hair cells and/or had internalized debris from
738 several hair cells was still classified as a single 'event.'
739 Subsequent image processing for display within figures was performed using Photoshop
740 and Illustrator software (Adobe).

741 ***Scanning electron microscopy***

742 To image hair-cell bundles, zebrafish larvae were exposed to strong water current
743 stimulus, then anesthetized in 0.12% tricaine in E3 and immediately fixed in 2.5%
744 glutaraldehyde in 0.1 M sodium cacodylate buffer (Electron Microscopy Sciences)
745 supplemented with 2 mM $CaCl_2$. Larvae were shipped overnight in fixative, then most of the
746 fixative (~90-95%) was removed, replaced with distilled water, and samples were stored at 4C.
747 Next, larvae were washed in distilled water (Gibco), dehydrated with an ascending series of
748 ethanol, critical point dried from liquid CO_2 (Tousimis Aurosamdri 815), mounted on adhesive
749 carbon tabs (TedPella), sputter coated with 5 nm of platinum (Leica EM ACE600), and imaged
750 on Hitachi S-4700 scanning electron microscope. Kinocilia diameter measurements were
751 performed using ImageJ.

752 ***Statistical analysis***

753 All statistical analyses were performed using Prism 8 (Graphpad Software Inc). Where
754 appropriate, datasets were confirmed for normality using the D'Agostino-Pearson test. Statistical
755 significance between multiple conditions with one independent variable was determined by one-
756 way ANOVA (normal distribution of data) or by a Kruskal-Wallis test (non-normal distribution of
757 data) and appropriate post-hoc tests. Statistical significance between multiple conditions with
758 two independent variables was determined by two-way ANOVA. Statistical significance between
759 two conditions was determined by an unpaired Student's *t* test or a Mann–Whitney U test, as
760 appropriate. The one-sample Wilcoxon test was used to calculate the difference between
761 observed and default value. Mixed model analysis was used to compare time-series data.
762 Based on the variance and effect sizes reported previously studies, the number of biological
763 replicates were suitable to provide statistical power to avoid both Type I and Type II error (Sebe
764 et al., 2017; Uribe et al., 2018).
765

766

767 References

768 Behra, M., Gallardo, V. E., Bradsher, J., Torrado, A., Elkahloun, A., Idol, J., . . . Burgess, S. M.
769 (2012). Transcriptional signature of accessory cells in the lateral line, using the
770 Tnk1bp1:EGFP transgenic zebrafish line. *BMC Dev Biol, 12*, 6. doi:10.1186/1471-213X-
771 12-6
772 Bhandiwad, A. A., Zeddies, D. G., Raible, D. W., Rubel, E. W., & Sisneros, J. A. (2013).
773 Auditory sensitivity of larval zebrafish (Danio rerio) measured using a behavioral
774 prepulse inhibition assay. *The Journal of experimental biology, 216*(Pt 18), 3504-3513.
775 doi:10.1242/jeb.087635
776 Bolte, S., & Cordelieres, F. P. (2006). A guided tour into subcellular colocalization analysis in
777 light microscopy. *J Microsc, 224*(Pt 3), 213-232. doi:10.1111/j.1365-2818.2006.01706.x
778 Buck, L. M., Winter, M. J., Redfern, W. S., & Whitfield, T. T. (2012). Ototoxin-induced cellular
779 damage in neuromasts disrupts lateral line function in larval zebrafish. *Hearing research,*
780 *284*(1-2), 67-81. doi:10.1016/j.heares.2011.12.001
781 Bullen, A., Anderson, L., Bakay, W., & Forge, A. (2019). Localized disorganization of the
782 cochlear inner hair cell synaptic region after noise exposure. *Biol Open, 8*(1).
783 doi:10.1242/bio.038547
784 Burgess, H. A., & Granato, M. (2007). Sensorimotor gating in larval zebrafish. *The Journal of*
785 *neuroscience : the official journal of the Society for Neuroscience, 27*(18), 4984-4994.
786 doi:10.1523/JNEUROSCI.0615-07.2007
787 Carpaneto Freixas, A. E., Moglie, M. J., Castagnola, T., Salatino, L., Domene, S., Marcovich, I.,
788 . . . Elgoyhen, A. B. (2021). Unraveling the Molecular Players at the Cholinergic Efferent
789 Synapse of the Zebrafish Lateral Line. *The Journal of neuroscience : the official journal*
790 *of the Society for Neuroscience, 41*(1), 47-60. doi:10.1523/JNEUROSCI.1772-20.2020
791 Carrillo, S. A., Anguita-Salinas, C., Pena, O. A., Morales, R. A., Munoz-Sanchez, S., Munoz-
792 Montecinos, C., . . . Allende, M. L. (2016). Macrophage Recruitment Contributes to
793 Regeneration of Mechanosensory Hair Cells in the Zebrafish Lateral Line. *J Cell*
794 *Biochem, 117*(8), 1880-1889. doi:10.1002/jcb.25487
795 Chen, Z., Kujawa, S. G., & Sewell, W. F. (2010). Functional roles of high-affinity glutamate
796 transporters in cochlear afferent synaptic transmission in the mouse. *Journal of*
797 *neurophysiology, 103*(5), 2581-2586. doi:10.1152/jn.00018.2010
798 Cho, S. I., Gao, S. S., Xia, A., Wang, R., Salles, F. T., Raphael, P. D., . . . Oghalai, J. S. (2013).
799 Mechanisms of hearing loss after blast injury to the ear. *PloS one, 8*(7), e67618.
800 doi:10.1371/journal.pone.0067618
801 Coffin, A. B., Kelley, M. W., Manley, G. A., & Popper, A. N. (2004). Evolution of sensory hair
802 cells. In G. A. Manley, R. R. Fay, & A. N. Popper (Eds.), *Evolution of the Auditory*
803 *System*. New York: Springer-Verlag.
804 Davies, C., Tingley, D., Kachar, B., Wenthold, R. J., & Petralia, R. S. (2001). Distribution of
805 members of the PSD-95 family of MAGUK proteins at the synaptic region of inner and
806 outer hair cells of the guinea pig cochlea. *Synapse, 40*(4), 258-268.
807 doi:10.1002/syn.1048
808 Dow, E., Jacobo, A., Hossain, S., Siletti, K., & Hudspeth, A. J. (2018). Connectomics of the
809 zebrafish's lateral-line neuromast reveals wiring and miswiring in a simple microcircuit.
810 *eLife, 7*. doi:10.7554/eLife.33988
811 Erickson, T., Pacentine, I. V., Venuto, A., Clemens, R., & Nicolson, T. (2019). The lhfpl5
812 Ohnologs lhfpl5a and lhfpl5b Are Required for Mechanotransduction in Distinct
813 Populations of Sensory Hair Cells in Zebrafish. *Front Mol Neurosci, 12*, 320.
814 doi:10.3389/fnmol.2019.00320

Faucherre, A., Pujol-Marti, J., Kawakami, K., & Lopez-Schier, H. (2009). Afferent neurons of the zebrafish lateral line are strict selectors of hair-cell orientation. *PloS one, 4*(2), e4477. doi:10.1371/journal.pone.0004477

Fernandez, K. A., Guo, D., Micucci, S., De Gruttola, V., Liberman, M. C., & Kujawa, S. G. (2020). Noise-induced Cochlear Synaptopathy with and Without Sensory Cell Loss. *Neuroscience, 427*, 43-57. doi:10.1016/j.neuroscience.2019.11.051

Gao, W. Y., Ding, D. L., Zheng, X. Y., Ruan, F. M., & Liu, Y. J. (1992). A comparison of changes in the stereocilia between temporary and permanent hearing losses in acoustic trauma. *Hearing research, 62*(1), 27-41. Retrieved from http://www.ncbi.nlm.nih.gov/pubmed/1429249

Glowatzki, E., & Fuchs, P. A. (2002). Transmitter release at the hair cell ribbon synapse. *Nature neuroscience, 5*(2), 147-154. doi:10.1038/nn796

Harris, J. A., Cheng, A. G., Cunningham, L. L., MacDonald, G., Raible, D. W., & Rubel, E. W. (2003). Neomycin-induced hair cell death and rapid regeneration in the lateral line of zebrafish (Danio rerio). *Journal of the Association for Research in Otolaryngology : JARO, 4*(2), 219-234. doi:10.1007/s10162-002-3022-x

Henry, W. R., & Mulroy, M. J. (1995). Afferent synaptic changes in auditory hair cells during noise-induced temporary threshold shift. *Hearing research, 84*(1-2), 81-90. Retrieved from http://www.ncbi.nlm.nih.gov/pubmed/7642458

Hickman, T. T., Smalt, C., Bobrow, J., Quatieri, T., & Liberman, M. C. (2018). Blast-induced cochlear synaptopathy in chinchillas. *Scientific reports, 8*(1), 10740. doi:10.1038/s41598-018-28924-7

Hirose, K., Discolo, C. M., Keasler, J. R., & Ransohoff, R. (2005). Mononuclear phagocytes migrate into the murine cochlea after acoustic trauma. *The Journal of comparative neurology, 489*(2), 180-194. doi:10.1002/cne.20619

Hirose, K., Rutherford, M. A., & Warchol, M. E. (2017). Two cell populations participate in clearance of damaged hair cells from the sensory epithelia of the inner ear. *Hearing research, 352*, 70-81. doi:10.1016/j.heares.2017.04.006

Hu, N., Rutherford, M. A., & Green, S. H. (2020). Protection of cochlear synapses from noise-induced excitotoxic trauma by blockade of Ca(2+)-permeable AMPA receptors. *Proceedings of the National Academy of Sciences of the United States of America, 117*(7), 3828-3838. doi:10.1073/pnas.1914247117

Husbands, J. M., Steinberg, S. A., Kurian, R., & Saunders, J. C. (1999). Tip-link integrity on chick tall hair cell stereocilia following intense sound exposure. *Hearing research, 135*(1-2), 135-145. doi:10.1016/s0378-5955(99)00101-x

Indzhykulian, A. A., Stepanyan, R., Nelina, A., Spinelli, K. J., Ahmed, Z. M., Belyantseva, I. A., . . . Frolenkov, G. I. (2013). Molecular remodeling of tip links underlies mechanosensory regeneration in auditory hair cells. *PLoS Biol, 11*(6), e1001583. doi:10.1371/journal.pbio.1001583

Jia, S., Yang, S., Guo, W., & He, D. Z. (2009). Fate of mammalian cochlear hair cells and stereocilia after loss of the stereocilia. *The Journal of neuroscience : the official journal of the Society for Neuroscience, 29*(48), 15277-15285. doi:10.1523/JNEUROSCI.3231-09.2009

Kaur, T., Clayman, A. C., Nash, A. J., Schrader, A. D., Warchol, M. E., & Ohlemiller, K. K. (2019). Lack of Fractalkine Receptor on Macrophages Impairs Spontaneous Recovery of Ribbon Synapses After Moderate Noise Trauma in C57BL/6 Mice. *Front Neurosci, 13*, 620. doi:10.3389/fnins.2019.00620

Kaur, T., Zamani, D., Tong, L., Rubel, E. W., Ohlemiller, K. K., Hirose, K., & Warchol, M. E. (2015). Fractalkine Signaling Regulates Macrophage Recruitment into the Cochlea and Promotes the Survival of Spiral Ganglion Neurons after Selective Hair Cell Lesion. *The*

Journal of neuroscience : the official journal of the Society for Neuroscience, 35(45), 15050-15061. doi:10.1523/JNEUROSCI.2325-15.2015

Kim, K. X., Payne, S., Yang-Hood, A., Li, S. Z., Davis, B., Carlquist, J., . . . Rutherford, M. A. (2019). Vesicular Glutamatergic Transmission in Noise-Induced Loss and Repair of Cochlear Ribbon Synapses. *The Journal of neuroscience : the official journal of the Society for Neuroscience, 39*(23), 4434-4447. doi:10.1523/JNEUROSCI.2228-18.2019

Kindt, K. S., Finch, G., & Nicolson, T. (2012). Kinocilia mediate mechanosensitivity in developing zebrafish hair cells. *Developmental cell, 23*(2), 329-341. doi:10.1016/j.devcel.2012.05.022

Kindt, K. S., & Sheets, L. (2018). Transmission Disrupted: Modeling Auditory Synaptopathy in Zebrafish. *Front Cell Dev Biol, 6*, 114. doi:10.3389/fcell.2018.00114

Kniss, J. S., Jiang, L., & Piotrowski, T. (2016). Insights into sensory hair cell regeneration from the zebrafish lateral line. *Curr Opin Genet Dev, 40*, 32-40. doi:10.1016/j.gde.2016.05.012

Kujawa, S. G., & Liberman, M. C. (2009). Adding insult to injury: cochlear nerve degeneration after "temporary" noise-induced hearing loss. *The Journal of neuroscience : the official journal of the Society for Neuroscience, 29*(45), 14077-14085. doi:10.1523/JNEUROSCI.2845-09.2009

LeMasurier, M., & Gillespie, P. G. (2005). Hair-cell mechanotransduction and cochlear amplification. *Neuron, 48*(3), 403-415. doi:10.1016/j.neuron.2005.10.017

Levi, R., Akanyeti, O., Ballo, A., & Liao, J. C. (2015). Frequency response properties of primary afferent neurons in the posterior lateral line system of larval zebrafish. *Journal of neurophysiology, 113*(2), 657-668. doi:10.1152/jn.00414.2014

Ma, E. Y., Rubel, E. W., & Raible, D. W. (2008). Notch signaling regulates the extent of hair cell regeneration in the zebrafish lateral line. *The Journal of neuroscience : the official journal of the Society for Neuroscience, 28*(9), 2261-2273. doi:10.1523/JNEUROSCI.4372-07.2008

McHenry, M. J., Feitl, K. E., Strother, J. A., & Van Trump, W. J. (2009). Larval zebrafish rapidly sense the water flow of a predator's strike. *Biol Lett, 5*(4), 477-479. doi:10.1098/rsbl.2009.0048

Merchan-Perez, A., & Liberman, M. C. (1996). Ultrastructural differences among afferent synapses on cochlear hair cells: correlations with spontaneous discharge rate. *The Journal of comparative neurology, 371*(2), 208-221. doi:10.1002/(SICI)1096-9861(19960722)371:2<208::AID-CNE2>3.0.CO;2-6

Nair, A., Azatian, G., & McHenry, M. J. (2015). The kinematics of directional control in the fast start of zebrafish larvae. *The Journal of experimental biology, 218*(Pt 24), 3996-4004. doi:10.1242/jeb.126292

Nordmann, A. S., Bohne, B. A., & Harding, G. W. (2000). Histopathological differences between temporary and permanent threshold shift. *Hearing research, 139*(1-2), 13-30. Retrieved from http://www.ncbi.nlm.nih.gov/pubmed/10601709

Nüsslein-Volhard, C., & Dahm, R. (2002). *Zebrafish : a practical approach* (1st ed.). Oxford: Oxford University Press.

Obholzer, N., Wolfson, S., Trapani, J. G., Mo, W., Nechiporuk, A., Busch-Nentwich, E., . . . Nicolson, T. (2008). Vesicular glutamate transporter 3 is required for synaptic transmission in zebrafish hair cells. *The Journal of neuroscience : the official journal of the Society for Neuroscience, 28*(9), 2110-2118. doi:10.1523/JNEUROSCI.5230-07.2008

Olivari, F. A., Hernandez, P. P., & Allende, M. L. (2008). Acute copper exposure induces oxidative stress and cell death in lateral line hair cells of zebrafish larvae. *Brain research, 1244*, 1-12. doi:10.1016/j.brainres.2008.09.050

Puel, J. L., Ruel, J., Gervais d'Aldin, C., & Pujol, R. (1998). Excitotoxicity and repair of cochlear synapses after noise-trauma induced hearing loss. *Neuroreport, 9*(9), 2109-2114. Retrieved from http://www.ncbi.nlm.nih.gov/pubmed/9674603

Qiu, X., & Muller, U. (2018). Mechanically Gated Ion Channels in Mammalian Hair Cells. *Frontiers in cellular neuroscience, 12*, 100. doi:10.3389/fncel.2018.00100

Ridler, T. W. C., S. (1978). Picture Thresholding Using an Iterative Selection Method. *3EEE TRANSACTIONS ON SYSTEMS, MAN, AND CYBERNETICS*(8), 630 - 632. doi:https://doi.org/10.1109/TSMC.1978.4310039

Roca, F. J., & Ramakrishnan, L. (2013). TNF dually mediates resistance and susceptibility to mycobacteria via mitochondrial reactive oxygen species. *Cell, 153*(3), 521-534. doi:10.1016/j.cell.2013.03.022

Romero-Carvajal, A., Navajas Acedo, J., Jiang, L., Kozlovskaja-Gumbriene, A., Alexander, R., Li, H., & Piotrowski, T. (2015). Regeneration of Sensory Hair Cells Requires Localized Interactions between the Notch and Wnt Pathways. *Developmental cell, 34*(3), 267-282. doi:10.1016/j.devcel.2015.05.025

Schneider, C. A., Rasband, W. S., & Eliceiri, K. W. (2012). NIH Image to ImageJ: 25 years of image analysis. *Nat Methods, 9*(7), 671-675. doi:10.1038/nmeth.2089

Sebe, J. Y., Cho, S., Sheets, L., Rutherford, M. A., von Gersdorff, H., & Raible, D. W. (2017). Ca(2+)-Permeable AMPARs Mediate Glutamatergic Transmission and Excitotoxic Damage at the Hair Cell Ribbon Synapse. *The Journal of neuroscience : the official journal of the Society for Neuroscience, 37*(25), 6162-6175. doi:10.1523/JNEUROSCI.3644-16.2017

Sheets, L., Kindt, K. S., & Nicolson, T. (2012). Presynaptic CaV1.3 channels regulate synaptic ribbon size and are required for synaptic maintenance in sensory hair cells. *The Journal of neuroscience : the official journal of the Society for Neuroscience, 32*(48), 17273-17286. doi:10.1523/JNEUROSCI.3005-12.2012

Sheets, L., Trapani, J. G., Mo, W., Obholzer, N., & Nicolson, T. (2011). Ribeye is required for presynaptic Ca(V)1.3a channel localization and afferent innervation of sensory hair cells. *Development, 138*(7), 1309-1319. doi:10.1242/dev.059451

Shi, L., Liu, L., He, T., Guo, X., Yu, Z., Yin, S., & Wang, J. (2013). Ribbon synapse plasticity in the cochleae of Guinea pigs after noise-induced silent damage. *PloS one, 8*(12), e81566. doi:10.1371/journal.pone.0081566

Song, Q., Shen, P., Li, X., Shi, L., Liu, L., Wang, J., . . . Yin, S. (2016). Coding deficits in hidden hearing loss induced by noise: the nature and impacts. *Scientific reports, 6*, 25200. doi:10.1038/srep25200

Toro, C., Trapani, J. G., Pacentine, I., Maeda, R., Sheets, L., Mo, W., & Nicolson, T. (2015). Dopamine Modulates the Activity of Sensory Hair Cells. *The Journal of neuroscience : the official journal of the Society for Neuroscience, 35*(50), 16494-16503. doi:10.1523/JNEUROSCI.1691-15.2015

Trapani, J. G., & Nicolson, T. (2010). Physiological recordings from zebrafish lateral-line hair cells and afferent neurons. *Methods in cell biology, 100*, 219-231. doi:10.1016/B978-0-12-384892-5.00008-6

Uribe, P. M., Villapando, B. K., Lawton, K. J., Fang, Z., Gritsenko, D., Bhandiwad, A., . . . Coffin, A. B. (2018). Larval Zebrafish Lateral Line as a Model for Acoustic Trauma. *eNeuro, 5*(4). doi:10.1523/ENEURO.0206-18.2018

Wagner, E. L., & Shin, J. B. (2019). Mechanisms of Hair Cell Damage and Repair. *Trends in neurosciences, 42*(6), 414-424. doi:10.1016/j.tins.2019.03.006

Wan, G., Gomez-Casati, M. E., Gigliello, A. R., Liberman, M. C., & Corfas, G. (2014). Neurotrophin-3 regulates ribbon synapse density in the cochlea and induces synapse regeneration after acoustic trauma. *eLife, 3*. doi:10.7554/eLife.03564

Wang, H., Yin, S., Yu, Z., Huang, Y., & Wang, J. (2011). Dynamic changes in hair cell stereocilia and cochlear transduction after noise exposure. *Biochem Biophys Res Commun, 409*(4), 616-621. doi:10.1016/j.bbrc.2011.05.049

Wang, X., Zhu, Y., Long, H., Pan, S., Xiong, H., Fang, Q., . . . Sha, S. H. (2018). Mitochondrial Calcium Transporters Mediate Sensitivity to Noise-Induced Losses of Hair Cells and Cochlear Synapses. *Front Mol Neurosci, 11*, 469. doi:10.3389/fnmol.2018.00469

Warchol, M. E. (2019). Interactions between Macrophages and the Sensory Cells of the Inner Ear. *Cold Spring Harb Perspect Med, 9*(6). doi:10.1101/cshperspect.a033555

Warchol, M. E., Schrader, A., & Sheets, L. (2021). Macrophages Respond Rapidly to Ototoxic Injury of Lateral Line Hair Cells but Are Not Required for Hair Cell Regeneration. *Frontiers in cellular neuroscience, 14*, 613246. doi:10.3389/fncel.2020.613246

Weeg, M. S., Fay, R. R., & Bass, A. H. (2002). Directionality and frequency tuning of primary saccular afferents of a vocal fish, the plainfin midshipman (Porichthys notatus). *Journal of comparative physiology. A, Neuroethology, sensory, neural, and behavioral physiology, 188*(8), 631-641. doi:10.1007/s00359-002-0338-2

Wong, H. C., Zhang, Q., Beirl, A. J., Petralia, R. S., Wang, Y. X., & Kindt, K. (2019). Synaptic mitochondria regulate hair-cell synapse size and function. *eLife, 8*. doi:10.7554/eLife.48914

Wynn, T. A., & Vannella, K. M. (2016). Macrophages in Tissue Repair, Regeneration, and Fibrosis. *Immunity, 44*(3), 450-462. doi:10.1016/j.immuni.2016.02.015

Xiao, Y., Faucherre, A., Pola-Morell, L., Heddleston, J. M., Liu, T. L., Chew, T. L., . . . Lopez-Schier, H. (2015). High-resolution live imaging reveals axon-glia interactions during peripheral nerve injury and repair in zebrafish. *Dis Model Mech, 8*(6), 553-564. doi:10.1242/dmm.018184

Zhang, Q., Li, S., Wong, H. C., He, X. J., Beirl, A., Petralia, R. S., . . . Kindt, K. S. (2018). Synaptically silent sensory hair cells in zebrafish are recruited after damage. *Nature communications, 9*(1), 1388. doi:10.1038/s41467-018-03806-8

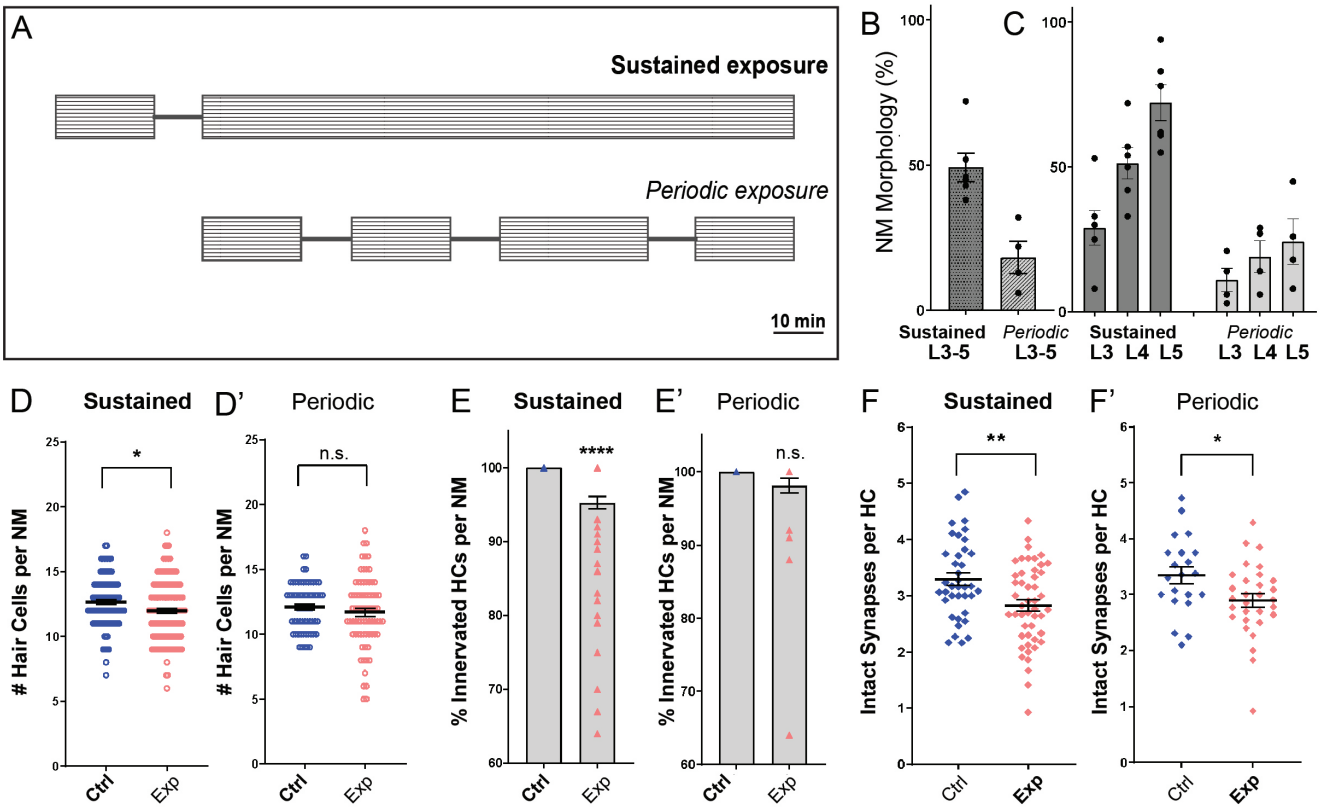

Supplemental Figure 1: Fish exposed to periodic stimulus have less mechanical damage to* neuromasts*, but still show significant synapse loss. **(A)** Schematic of the two exposure protocols. Sustained exposure was a 20 min. pulse followed by 120 minutes uninterrupted mechanical overstimulation; periodic exposure was 90 min. exposure with intermittent 10 min. breaks totaling 120 minutes. **(B)** Periodic stimulus causes less neuromast disruption. Immediately following sustained exposure, 46% of exposed neuromasts showed a "disrupted" phenotype, whereas following a periodic exposure only 17% of the neuromasts appeared "disrupted" (Unpaired t-test **P=0.0034). **(C)** Position of the neuromast along the tail was also associated with vulnerability to disruption with both sustained and periodic stimulation. **(D-D')** Hair cell number per neuromast following exposure. With periodic exposure, the number of hair cells was comparable to control (Unpaired t-test, *P=0.0125 sustained , P=0.9916 periodic). **(E-E')** % of neuromast hair cells innervated. There was no significant reduction in afferent innervation of neuromast hair cells (One sample Wilcoxon test, ****P<0.0001 sustained, P=0.0625 periodic). **(F-F')** Number of intact synapses per neuromast. There is significant loss of synapses with both periodic and sustained exposures (*P=0.0245 periodic; **P=0.0036 sustained).

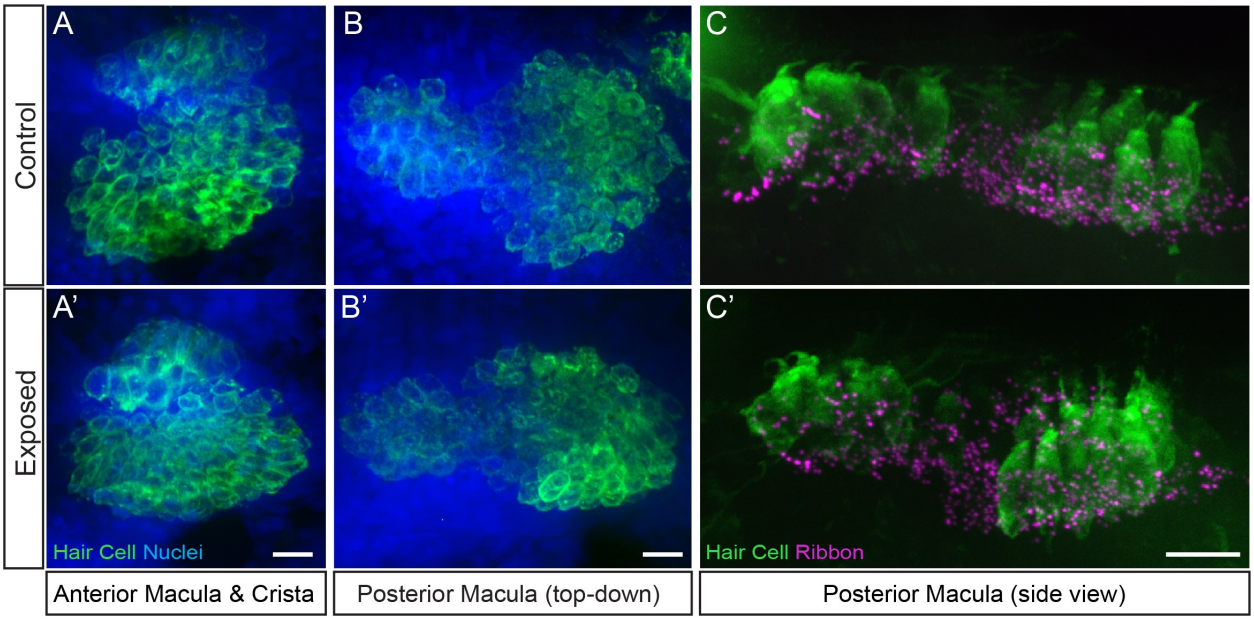

996

Supplemental Figure 2: Hair cell organs of the ear appeared undamaged in larvae exposed to sustained stimulus. Representative maximum intensity images of hair cell organs in the ears of control **(A-C)** and larvae exposed to sustained strong current stimulus **(A'-C')**. Hair cells in A-B were immunolabeled with an antibody against Otoferlin; posterior macula in C were immunolabled with antibodies against Parvalbumin to label hair cells and CtBP to label synaptic ribbons. Scale bars: 10µm

997

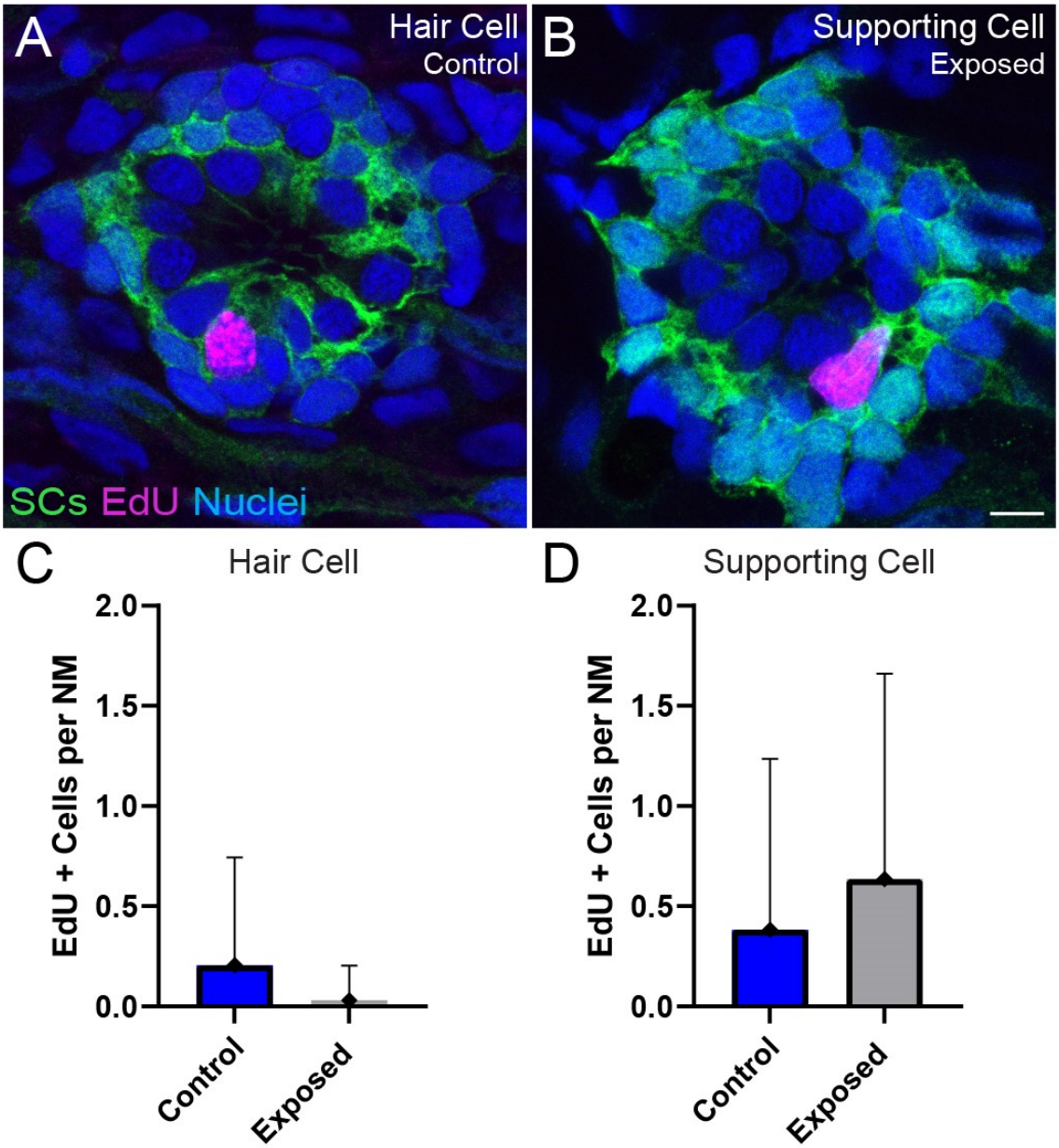

998

Supplemental Figure 3: Exposed* neuromast*s show a modest increase in supporting cell proliferation following sustained stimulation. **(A,B)** Representative cross-section images of EdU (magenta) labeling of proliferating neuromast cells. Fish were exposed to EdU for 4 hours following exposure. **(A)** EdU labeling of neuromast hair cell not co-localized with GFP. **(B)** EdU labeling colocalized with supporting cell GFP label. Scale bars: 5μm **(C-D)** Average number of EdU+ hair cell (C) or supporting cells (D) per neuromasts. The average number of EdU+ supporting cells were significantly greater than 0 in all neuromasts, with a modest increase in exposed neuromasts (Wilcoxon Rank Test: **P=0.0078, ***P=0.0005).

999

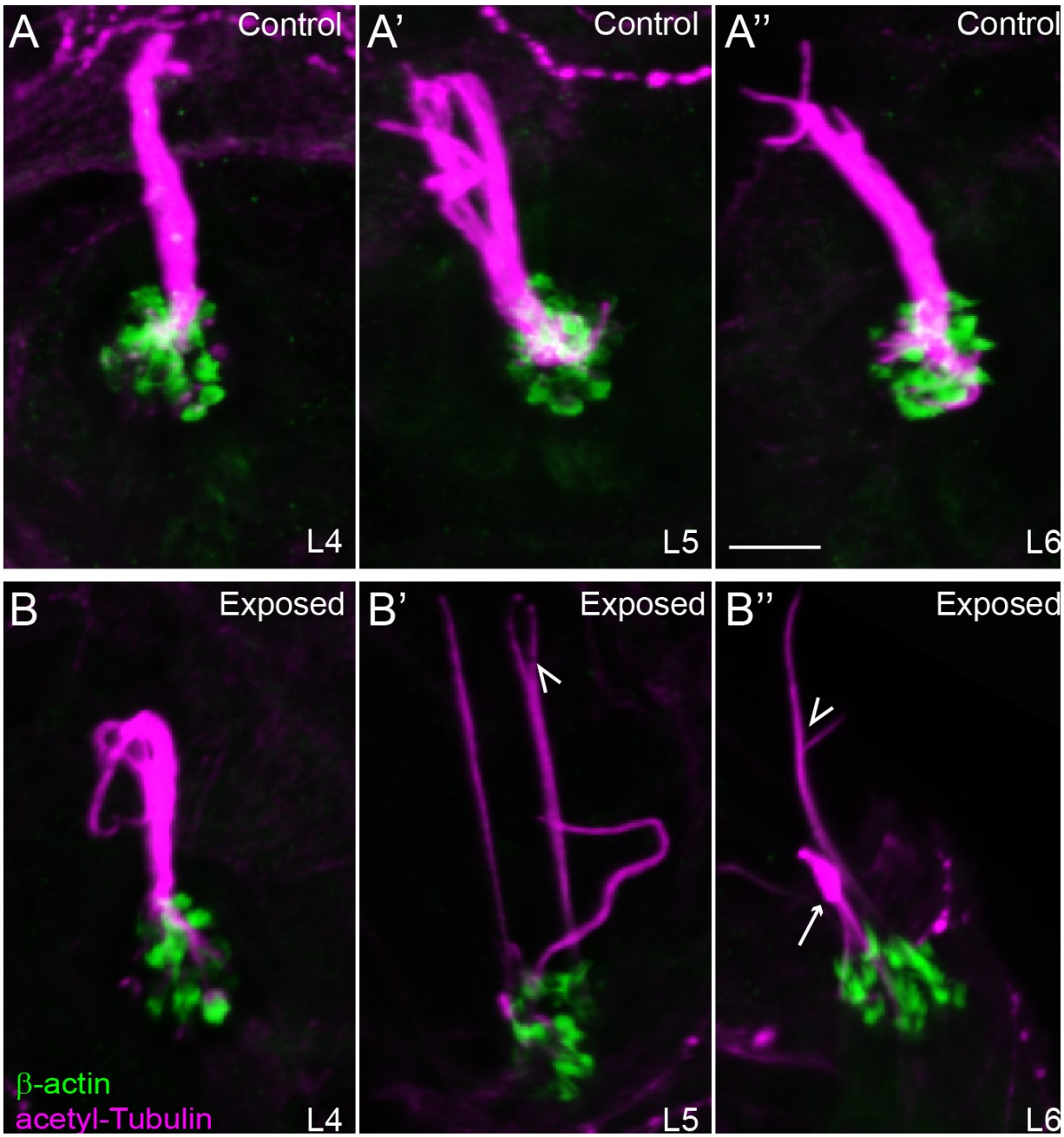

1000

Supplemental Figure 3: Exposed* neuromast*s show a modest increase in supporting cell proliferation following sustained stimulation. **(A,B)** Representative cross-section images of EdU (magenta) labeling of proliferating neuromast cells. Fish were exposed to EdU for 4 hours following exposure. **(A)** EdU labeling of neuromast hair cell not co-localized with GFP. **(B)** EdU labeling colocalized with supporting cell GFP label. Scale bars: 5μm **(C-D)** Average number of EdU+ hair cell (C) or supporting cells (D) per neuromasts. The average number of EdU+ supporting cells were significantly greater than 0 in all neuromasts, with a modest increase in exposed neuromasts (Wilcoxon Rank Test: **P=0.0078, ***P=0.0005).

1001

1002

1003 **Supplemental Movies**

1004 Swimming behavior of 7-day-old larvae during exposure to the strong water current stimulus
1005 shown in Figure 2 over 500ms (1000 fps/ 500 frames).

1006

1007 **Movie S1:** Swimming behavior of control fish with intact lateral line organs. Magenta circle
1008 indicates a fish prior to a “fast escape” response.

1009

1010 **Movie S2:** Swimming behavior of larvae whose lateral-line neuromasts were ablated with
1011 $CuSO_4$. Magenta circles indicate larvae that were swept into the waves and could no longer
1012 tracked.

1013

1014

"Mechanical overstimulation causes acute injury and synapse loss followed by fast recovery in lateral-line neuromasts of larval zebrafish"

Response to Preprint Peer Review comments

We would like to thank the reviewers for their thoughtful and thorough critique of our manuscript. In this resubmission, we added important additional data and restructured our manuscript to reflect as many of the recommendations as possible. Additionally, we have added experiments to define the cellular mechanisms underlying observed damage following mechanical injury.

The most significant additions of new data include:

- Further experiments demonstrating block of glutamate clearance exacerbates stimulus-induced hair-cell synapse loss.
- Analysis of neuromast disruption in *lhfpl5b* mutant null larvae showing mechanical displacement. Lhfpl5b mediates mechanosensitivity in lateral-line hair cells, allowing us to determine whether mechanotransduction is required for mechanical disruption of neuromasts.
- Testing the vibratory stimulus at various frequencies to confirm the optimal frequency to induce acute, generally sub-lethal damage to lateral-line hair cells is 60 Hz.
- Assessment of neuromast supporting cell and hair cell proliferation following mechanical overstimulation.
- Quantitative analysis of kinocilia SEM and confocal images of hair bundles in control and stimulus exposed fish.

Individual comments are addressed as outlined below.

Reviewer 1:

- The authors use a vertically-oriented Brüel+Kjær LDS Vibrator to deliver a 60 Hz vibratory stimulus to damage lateral line hair cells. It is not made clear on why this frequency was selected. Did the authors choose this frequency because they screened a number of frequencies and this is the one that did the most damage to hair cells or was it chosen for another reason? Or, do all frequencies do the same amount of damage? The authors should screen a number of frequencies and choose the stimulus that does the most damage to hair cells. This would set the field in the best direction, should members of the community attempt this new technique. It is not necessary to repeat all of the experiments, but the authors should show which frequencies are best for inducing damage.

The frequency selected for mechanical overexposure of lateral-line organs was based on previous studies showing 60 Hz to be within the optimal upper frequency range of mechanical sensitivity of superficial posterior lateral-line neuromasts, with maximal response between 10-60 Hz, but a suboptimal frequency for hair cells of the anterior macula in the ear (Weeg and Bass 2002, Trapani et al, 2009, Levi et al, 2015). To confirm that 60 Hz was the optimal frequency to induce damage, we tested 45, 60, and 75 Hz at comparable intensities. We observed at 75 Hz no apparent damage to lateral

line neuromasts while 45 Hz at a comparable intensity proved toxic i.e. it was lethal to the fish. We have updated the Results and Method Details to include our rationale for choosing 60 Hz.

- The SEM images of the hair bundle are beautiful and do show damage to the hair bundle, but historically speaking older studies in mammals have shown that the actin core of the stereocilia is damaged. It would be critical to know if this was the case. Showing damage to the kinocilium and stereocilia splaying is a start, but readers of eLife would need to know if the actin cores are damaged. So, TEM should be used to find damage to the actin cores of stereocilia.

Our main goal of this initial manuscript was to survey morphological and functional changes in mechanically injured lateral line organs with an emphasis on inflammation and synapse loss. We agree TEM studies showing damage to the actin core of the stereocilia will be important to determine whether mechanical damage to neuromast hair bundles fully mimics mammalian stereocilia damage, but these experiments will require significant time to perform and optimize. We have expanded our analysis of hair-bundle morphology in this study and intend to pursue deeper analysis of hair bundle damage, i.e. examination of the stereocilia actin core, in future follow-up studies.

- I think the use of "Noise-exposed lateral line" as a term for mechanically overstimulated lateral line hair cells is not correct and could be misleading. The lateral line senses water motion not sound as the word noise would imply. Calling the stimulus "noise" should be removed throughout.

We have removed the term “noise” throughout the manuscript and replaced it with either “strong water current stimulus” or “mechanical overstimulation” where appropriate.

- Decreases in mechanotransduction are shown by dye entry. These results should be strengthened using microphonic potentials to determine the extent of damage. This experiment is not necessary but would improve the quality of the document.

While we agree that microphonic recordings would provide further support for reduced mechanotransduction, quantitative FM1-43 uptake in zebrafish lateral line hair cells is a well-established proxy for microphonic measurements. In a previous study using the same protocol utilized in our manuscript, FM1-43 labeling intensity was shown to directly correspond with microphonic amplitude (Toro et al, 2015). Moreover, the fixable analogue of FM1-43 (FM1-43FX) gave us comparable relative measurements of uptake as live FM1-43 and provided the additional advantage of high temporal resolution and the ability to simultaneously assay entire cohorts of control and overstimulated fish (which is not possible with microphonic measurements or live FM1-43 imaging), as we could expose groups of fish briefly to the dye at determined time intervals following overstimulation, then immediately place in fixative.

- In figure (2), PSD labeling is not clear.

We assume the reviewer meant PSD labeling in Figure 4 and we agree it is difficult to discern. We have changed the hair-cell label from gray to blue in the images so that the green PSD labeling is clear.

1105 *Minor comments*
1106 *- Page 2- "They transduce these stimuli though deflection of stereocilia....". Change*
1107 *"though" to "through".*
1108 *- Figure 1 legend add "be" between longer and tracked "could no longer tracked".*
1109
1110 Thank you for identifying these typos. They have been corrected.
1111
1112 *Reviewer 2:*
1113 *1. While the findings are carefully measured and described, the effects of insult on hair*
1114 *cells are relatively minor, with a change in hair cell number, extent of innervation or*
1115 *synapses per hair cell (Figs 3 and 4) in the range of 10% reduction compared to control.*
1116 *One potential value of the model would be to use it to discover underlying pathways of*
1117 *damage or screen for potential therapeutics. However with these modest changes it is*
1118 *not clear that there will be enough power to determine effects of potential interventions.*
1119 One advantage of the zebrafish model is the ability to overstimulate large cohorts of
1120 larvae, thereby providing enough power to uncover modest but significant changes
1121 resulting from moderate damage to hair cells. While not as well suited for unbiased
1122 large-scale screens of therapeutics, our overexposure protocol provides the opportunity
1123 to determine the role of specific cellular pathways (e.g. metabolic stress, inflammation,
1124 and glutamate excitotoxicity) in hair-cell damage and synapse loss following
1125 mechanically-induced damage via genetic or pharmacological manipulation of these
1126 pathways. Additionally, as the hair cell synapses fully repair following stimulus-induced
1127 loss, the zebrafish model has the potential for identifying novel pathways for repair
1128 through transcriptomic profiling (for an example, see Mattern et al, Front. Cell Dev. Biol.,
1129 2018). Cumulatively, these future experimental directions will provide important
1130 mechanistic information that could be used toward the development of targeted
1131 therapeutic interventions.
1132
1133 *2. The most dramatic phenotype after shaking is a physical displacement of hair cells,*
1134 *described as disrupted morphology. However it is not clear what the underlying cause of*
1135 *this change. Are only posterior neuromasts damaged in this way? Is it a wounding*
1136 *response as animals are exposed to an air interface during shaking? It is also not clear*
1137 *to what extent this displacement reveals more general principles of the effects of noise*
1138 *on hair cells. Additional discussion of underlying causes would be welcome.*
1139 We agree that the underlying causes of the physical displacement of posterior lateral-
1140 line neuromasts warranted further investigation and we have expanded appropriate
1141 sections of the results. To determine if excessive hair-cell activity plays a role in the
1142 displacement of neuromasts we have exposed *lhfpl5b* mutant—fish that have intact hair
1143 cell function in the ear, but no mechanotransduction in hair cells of the lateral line—to
1144 mechanical overstimulation. We observed comparable disruption of neuromasts lacking
1145 mechanotransduction, supporting that displacement of lateral-line hair cells is due to
1146 mechanical damage and does not require intact mechnotransduction. Further, when
1147 examining the adjacent supporting cells in disrupted neuromasts, we observed they are
1148 similarly displaced and elongated. We conclude that observed disruption of hair cells is
1149 a consequence of mechanical displacement of the entire neuromast organ. We have

1150 added additional discussion of this phenomenon to the Results and Discussion sections
1151 of the manuscript.
1152
1153 *3. Because afferent neurons innervate more than one neuromast and more than one*
1154 *hair cell per neuromast, measurements of innervation of neuromasts (Figure 3) or*
1155 *synapses per hair cell (Fig 4) cannot be assumed to be independent events. That is,*
1156 *changes in a single postsynaptic neuron may be reflected across multiple synapses,*
1157 *hair cells, and even neuromasts. This needs to be accounted for in experimental design*
1158 *for statistical analysis.*
1159 We agree that changes in single postsynaptic neurons, which innervate groups of hair
1160 cells of the same polarity within a neuromast, could be reflected across multiple
1161 synapses. Additionally, it is plausable that excitotoxic events at the postsynapse, while
1162 not contributing to apparent neurite retraction, could be contributing to synapse loss
1163 across multiple innervated hair cells. We have updated the manuscript to reflect the
1164 potential contribution of postsynaptic signaling to synapse loss and added experiments
1165 pharmacologically blocking glutamate uptake.
1166
1167 *4. The SEM analysis provides compelling snapshots of apical damage, but could be*
1168 *supplemented by quantitative analysis with antibody staining or transgenic lines where*
1169 *kinocilia are labeled. The amount of reduced FM1-43 labeling is one of the more*
1170 *dramatic effects of the shaking insult, suggesting widespread disruption to*
1171 *mechanotransduction that could be related to this apical damage. Further examination*
1172 *of the recovery of mechanotransduction would be interesting.*
1173 To supplement the SEM snapshots of severe apical damage, we have expanded the
1174 SEM image analysis with quantitative data on kinocilia morphology. We have also
1175 added confocal images of hair bundles using antibody labeling of acetylated tubulin in a
1176 transgenic line expressing β-actin-GFP in hair cells. We agree that correlative studies of
1177 mechanotransduction recovery relative to hair-bundle morphology would be interesting,
1178 and we intend to examine this question in a future follow-up study.
1179
1180 *5. A previous publication by Uribe et al.2018 describes a somewhat similar shaking*
1181 *protocol with somewhat different results - more long-lasting changes in hair cell number,*
1182 *presynaptic changes in synapses, etc. It would be worth discussing potential differences*
1183 *across the two studies.*
1184 We agree we did not adequately address the considerable differences between our
1185 mechanical damage protocol for the zebrafish lateral line and the damage protocol
1186 described by Uribe et al, 2018. We have provided a more direct comparison in the
1187 Results section and addressed the differences in our protocols in-depth in the
1188 Discussion section.
1189 Our damage protocol uses a stimulus within the known frequency range of lateral-line
1190 hair cells (60 Hz) that is applied to free-swimming larvae and evokes a behaviorally
1191 relevant response (fast start response). The damage is observable immediately
1192 following noise exposure, is specific to posterior lateral-line neuromasts, and appears to
1193 be rapidly repaired. Some features of the damage we observe—reduced
1194 mechanotransduction and hair-cell synapse loss—may correspond to mechanically
1195 induced damage of hair cell organs in other species. Notably, hair cell synapse loss in

1196 seemingly intact neuromasts is exacerbated by pharmacologically blocking synaptic
1197 glutamate clearance, supporting that the 60 Hz frequency stimulus is overstimulating
1198 neuromast hair cells directly and suggesting that the mechanism of synapse loss may
1199 be similar to inner hair cell synapse loss reported in mice following moderate noise
1200 exposures.
1201 By contrast, the damage protocol published by Uribe et al used ultrasonic transducers
1202 (40-kHz) to generate small, localized shock waves rather than directly stimulate
1203 neuromast hair cells. The damaged they reported—delayed hair-cell death and modest
1204 synapse loss with no effect on hair-cell mechanotransduction—was not apparent until
1205 48 hours following exposure and not specific to the lateral-line organ. Some of the
1206 features of the damage they observed—delayed onset apoptosis and hair-cell death—
1207 may correspond to damage reported in mice following blast injuries.
1208
1209 *Minor Comments:*
1210
1211 *6. Copper is potentially non-specific, described as neurotoxic. Are there other tests for*
1212 *lateral line-dependent effects on swimming/escape responses?*
1213 A previous study comparing the effect of various ototoxins in zebrafish determined
1214 exposure to low-dose $CuSO_4$ for 1 hour did not alter the acoustic escape response,
1215 which is similar to the fast start response we observed but evoked by higher frequency
1216 stimulation (100-500 Hz) of the anterior macula of inner ear (Buck et al, Hearing
1217 Research, 2012) We have added this information and citation to the manuscript.
1218 *7. Statistics for quantified differences in behaviors in Figure 1 are missing.*
1219 We have added the statistics to the manuscript.
1220
1221 *8. Micrograph examples of neuromast displacement in addition to the schematic would*
1222 *be helpful in describing the phenotype.*
1223 We have added representative confocal images of neuromast morphology to Figure 2. In
1224 addition, we've supplemented our images of neuromast hair cells additional labeling
1225 which shows similar displacement of the supporting cells in disrupted neuromasts.
1226 *9. Define error bars in figure legends. What are additional points in 3E?*
1227 The error bars have been defined as either standard error of the mean (SEM) or
1228 standard deviation (SD) in the figure legends. In 3E each point represents the percentage
1229 of hair cells with afferent innervation in a single neuromast; multiple individual points in
1230 the Control and Normal Exposed appear as one because the symbols all overlap at 100%
1231 innervated. This information has been added to the Figure legend.
1232 *10. Are differences in hc number in Fig 6 significant?*
1233 The differences in hair-cell number in Fig 6 were significant at 0 and 2 hours post
1234 exposure (Mixed-effects analysis: $^{**}P<0.003$). The appropriate statistical analysis has
1235 been added to this figure and to the text.
1236
1237 *11. Were hair cell changes in the ear observed, as reported by Uribe et al?*
1238 We did not observe hair cell changes in either the posterior or anterior macula in the
1239 ears of overexposed larvae. An additional supplemental figure (Supplemental Fig. 2)
1240 and a description in the results have been added to the manuscript.
1241

1242 *Reviewer 3:*
1243 *• As the authors point out, zebrafish hair cells can be regenerated. With that in mind,*
1244 *and to make the relevance for mammalian hair cell repair clear, a clear distinction*
1245 *between mechanisms mediated by "repair" or "regeneration" needs to be made. The*
1246 *authors discuss that proliferative hair cell generation can be excluded based on the*
1247 *short time period, but suggest that transdifferentiation might be involved. Recovery of*
1248 *neuromast hair cell number occurs within the same 2 hour period in which neuromast*
1249 *morphology and hair cell function improved, making it difficult to determine the extent to*
1250 *which "regeneration" contributed to the recovery. The amount of transdifferentiation has*
1251 *to be shown experimentally (lineage tracing?).*
1252 We agree that the distinction between "repair" and "regeneration" needs to be made
1253 when discussing this model of mechanical damage to zebrafish hair cell organs. We
1254 have tried to clarify that most of what we observe regarding recovery—restoration of
1255 neuromast shape, mechanostransduction, afferent contacts, and synapse number —
1256 reflect mechanisms of repair following mechanical damage (and, in the case of synapse
1257 loss, overstimulation) rather than regeneration. However, one feature of damage that
1258 may reflect rapid regeneration is restoration of hair cells number following mechanical
1259 injury. To experimentally determine whether proliferation contributed to hair cell
1260 generation, we assessed the incorporation of the thymidine analog EdU during a 4 hour
1261 recovery following mechanical overexposure in a transgenic line expressing GFP in
1262 neuromast supporting cells and observe a modest but not statistically significant increase
1263 in the number of proliferating supporting cells in neuromasts exposed to strong current
1264 stimulus, suggesting recovery of lost hair cells is not primarily due to renewed
1265 proliferation.
1266
1267 The number of hair cells that are lost and recover within several hours are low, i.e.,
1268 typically ~1 hair cell/neuromast. We observed this consistently in all of our experiments,
1269 but the mechanisms responsible are not clear. Based on previous studies of hair cell
1270 regeneration in the lateral line, the recovery time appears too rapid to be caused by
1271 renewed proliferation, a notion that is further supported by our Edu studies. On the other
1272 hand, it is possible that a few supporting cells may undergo the initial phases of
1273 phenotypic change into hair cells during this short time period, and we speculate that
1274 such transdifferentiation may be responsible for the observed recovery. We should
1275 emphasize that this is a new observation and, at present, we do not fully understand the
1276 underlying mechanism. However, the focus of the present study is on mechanical
1277 damage, synaptic loss, and subsequent repair. We believe that it is important to report
1278 our consistent findings of low level hair cell loss and recovery, but a detailed
1279 characterization of the mechanism would require considerable effort and would best be
1280 the topic of a future study.
1281
1282 *• The classification of "normal" vs "disrupted" is vague and not quantitative. The*
1283 *examples shown in the paper seem to be quite clear-cut, but this reviewer doubts that*
1284 *was the case throughout all analyzed samples. Formulate clear benchmarks and criteria*
1285 *for the disrupted phenotype (even when blind analysis is performed).*
1286 We have defined measurable criteria for "normal" vs "disrupted" neuromasts that we
1287 have added to the Method Details section: “We defined exposed neuromast morphology

1288 as “normal” when hair cells appeared radially organized with a relatively uniform shape
1289 and size, with ≤7 µm difference observed when comparing the lengths from apex to
1290 base of an opposing pair of anterior/posterior hair cells. Length was measured from a
1291 fixed point at the center of the hair bundle to the basolateral end of each opposing hair
1292 cell. We defined neuromasts as “disrupted” when hair cells appeared elongated and
1293 displaced to one side, with >7 µm difference observed when comparing the lengths of
1294 an opposing pair of anterior/posterior hair cells. Generally, the apical ends of the hair
1295 cells were displaced posteriorly, with the basolateral ends oriented anteriorly.”
1296
1297 • *Sustained and periodic exposure: These two exposure protocols not only differ with*
1298 *respect to sustained vs periodic, they also differ in total exposure time (Fig 2B). This*
1299 *complicates the interpretation, especially considering the authors own finding that a pre-*
1300 *exposure is protective.*
1301 To clarify—pre-exposure was not protective to hair-cell survival. Rather, in preliminary
1302 experiments, pre-exposure appeared to reduce larval mortality, and we have clarified
1303 that observation in the text of the Results and the Methods Details sections. We agree
1304 with the reviewer that comparing the two protocols based on differences in time
1305 distribution is complicated in that they also differ in total exposure time. For the purpose
1306 of clarity, we now focus on the sustained exposure in the main figures and created
1307 supplemental figures for the reduced damage still observed using periodic exposure,
1308 specifying that reduced damage may be the result of periodic time distribution of
1309 stimulus and/or less cumulative time exposed to the stimulus.
1310
1311 • *The data on the mitochondrial ROS aspect seems not well integrated into the overall*
1312 *story.*
1313 We agree that the ROS story was not well integrated and incomplete. We have
1314 removed the data describing *mpv17-/-* mutants and mitochondrial disfunction from this
1315 manuscript. A more comprehensive report of *mpv17-/-* mutant mitochondrial function
1316 and morphological analysis of neuromasts following noise exposure will be described in
1317 a follow-up manuscript.
1318
1319 • *It is surprising that the hair bundle morphology was not assessed after recovery. This*
1320 *is crucial. Overall, it would be good to see some quantification of the SEM data, e.g.*
1321 *kinocilia length and number of splayed bundles.*
1322 We have expanded the SEM image analysis to quantitatively access kinocilia
1323 morphology following exposure. We agree that assessment of recovery using live-
1324 imaging of hair bundles paired with subsequent SEM analysis will be informative, and
1325 we intend to perform those experiments in a future study.
1326
1327 • *Behavioral recovery (measured as number of "fast start" responses) was also not*
1328 *assessed. This is essential for determining the functional relevance of the recovery.*
1329 We attempted to measure behavior recovery of lateral-line function by measuring “fast-
1330 start” responses immediately and several hours after recovery, and discovered that i)
1331 strong water current provided stimulation that was too intense to reveal subtle
1332 behavioral changes following lateral-line damage and recovery, and ii) when testing
1333 larvae immediately following sustained strong current exposures, it was difficult to

1334 discern if fewer “fast-start” responses were due to lateral-line organ damage or larval
1335 fatigue.
1336 We agree that behavioral recovery is important to assay but acknowledge assessing
1337 lateral-line mediated behavior following mechanical damage will require a more
1338 sensitive testing paradigm that stimulates the lateral-line sensory organ with a relatively
1339 gentile, calibrated water flow stimulus. We are currently performing a follow-up study to
1340 this paper using a testing paradigm developed by a postdoctoral associate in our lab
1341 (Kyle Newton) that analyses subtle changes in larval orientation to water flow
1342 (rheotaxis) mediated by the lateral-line organ. Using this behavior paradigm, we will
1343 directly correlate morphological and functional recovery over time.
1344
1345 *• This reviewer is not yet convinced that this damage model displays enough*
1346 *commonalities to mammalian noise damage to justify the ubiquitous use of the term*
1347 *"noise" throughout the manuscript. It would be more prudent to use a more careful term*
1348 *along the lines of "mechanical overstimulation-induced damage".*
1349 We have removed the term “noise” throughout the manuscript and replaced it with either
1350 “strong water current stimulus” or “mechanical overstimulation” where appropriate.
1351
1352 *• How was afferent innervation quantified? Just counting GFP labeled contacts to hair*
1353 *cells?*
1354 Innervation of neuromast hair cells was quantified during blinded analysis by scrolling
1355 through confocal z-stacks of each neuromast (step size 0.3 µm) containing hair cell and
1356 afferent labeling and identifying hair cells that were not directly contacted by an afferent
1357 neuron i.e. no discernable space between the hair cell and the neurite. Hair cells that
1358 were identified as no longer innervated showed measurable neurite retraction; there
1359 was generally >0.5 µm distance between a retracted neurite and hair cell. We have
1360 added this information to the Methods Detail section.
1361
1362 *There was also inconsistency in the use of two variations of the mechanical damage*
1363 *protocol, the time points at which repair was assessed, and whether the damage was*
1364 *quantified in all neuromasts or in normal vs. disrupted neuromasts separately, making*
1365 *the data difficult to interpret.*
1366 We have revised our figure legends to clearly indicate when we are assessing damage
1367 in all exposed neuromasts (pooled) to control vs. comparative analysis of normal vs.
1368 disrupted neuromasts relative to control. In addition, we now focus on the sustained
1369 exposure in the main figures, which was the exposure protocol used for the time points
1370 in which repair and recovery were assessed.
1371
1372 *Minor comments:*
1373
1374 *• Please discuss the implications of why you think there was only a significant reduction*
1375 *in synapses only in "normal" neuromasts and not "disrupted". Maybe because more cell*
1376 *death occurred in disrupted neuromasts, especially in cells with more synapse loss?*
1377 We believe the synapse loss we observe in “normal” neuromasts is a consequence of
1378 hair-cell overstimulation, which is supported by our observation that blocking glutamate
1379 uptake significantly worsens synapse loss specifically in neuromasts with overall intact

1380 morphology. Speculatively, the mechanical damage observed in “disrupted” neuromasts
1381 (damaged kinocilia, splayed hair bundles, severely reduced FM1-43) may result in
1382 correspondingly impaired synaptic activity, thereby providing protection from synapse
1383 loss driven by excess stimulation.
1384
1385 • *Clarify whether data in figures 7 and 8 were derived from sustained noise protocol.*
1386 We have clarified that the data in figures 7 and 8 were derived from sustained noise
1387 protocol in the figure legends and the manuscript.
1388
1389 • *Why was the sustained protocol used for experiments looking at repair? Wouldn't it be*
1390 *more clear to use the periodic protocol, which results in less hair cell death, in which*
1391 *case most of the repair seen would be due to direct repair, rather than*
1392 *transdifferentiation of SCs to replace damaged hair cells?*
1393 We chose to focus on sustained mechanical exposure for this initial study characterizing
1394 mechanical injury to the lateral line because it produced more severe neuromast
1395 damage with mostly comparable phenotypes to the periodic protocol.
1396
1397 • *A few representative images demonstrating the presence of tip links in both groups*
1398 *would be important to support the authors claims. Quantification may be difficult, but it*
1399 *would be surprising if tip links weren't damaged immediately following mechanical*
1400 *damage.*
1401 One of the major issues we encountered when preparing our samples for SEM was the
1402 removal of the gelatinous cupula that covers the apical end of the neuromasts. We
1403 discovered that higher doses of the fish anesthetic Tricaine (0.12%) had the effect of
1404 dissolving the cupula but also made intact hair bundles more difficult to identify. Below
1405 (pg. 52) are examples of lower dose tricaine-treated neuromast hair bundles in control
1406 fish—notice the gelatinous gunk covering the stereocilia. On the lower right are arrows
1407 indicating what may be tip links. We hope to further investigate tip link loss and
1408 recovery, but it will first require a careful titration of tricaine concentration that would
1409 yield a higher tip link presence in control samples.

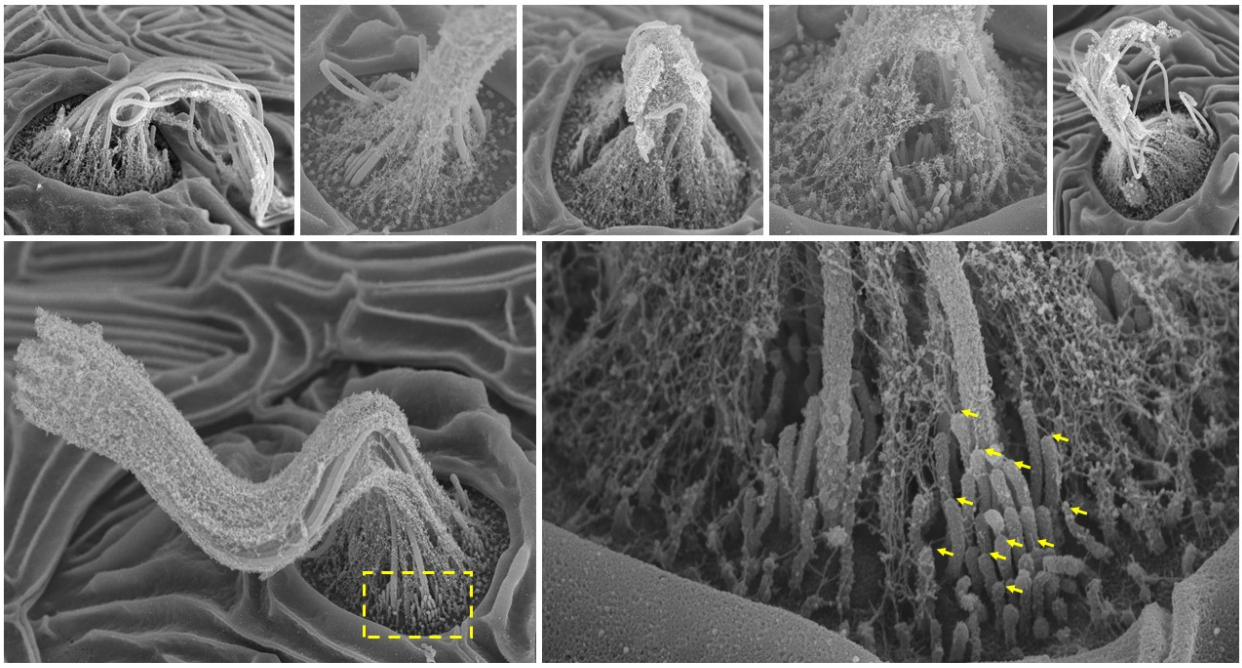

• Display statistical analysis in graphs in Figure 2.
Statistical analysis in Figure 2 F have been added.

• Describe statistics used to analyze data presented in Figure 6 in results section and display the results of this analysis in the figure.
We used mixed-effects modeling to analyze inflammation time series data. The results of these analyses are now displayed in Figure 6.

• Display statistical analysis in graphs in Figure 7.
Statistical analysis is displayed in graphs in Figure 7.

• Discuss differences between mammals and fish. Speculate about why fish might be more efficient than mammals at repairing sublethal damage when damaged cells could be easily replaced. Is this surprising?
We include in the Discussion section that the rapid recovery we observe in mechanically injured lateral-line organs may reflect the recovery from mild to moderate neuromast damage that occurs in this externally localized sensory organ that is directly exposed to the fish's environment and therefore continuously vulnerable to injury. The superficial lateral line's direct exposure to the environment may require more robust mechanisms for repair, in contrast to hair cell organs of mammals which are encased in bone.

• Discuss in more depth the debate about synapse repair in mammals and whether the results in this manuscript are similar to those studies showing repair in rodents.
While we did not go into depth on the debate about synaptic repair in different mammalian model systems, we did acknowledge ribbon synapse repair in the cochlea following noise trauma has been reported as partial in some mammalian models (i.e. a

subset of synapses are permanently lost) and the underlying mechanisms of repair appear to involve glutamate signaling, inflammation, and neurotrophic factors. As we observe complete hair-cell synaptic recovery, our reported zebrafish model of hair cell mechanical overstimulation may provide further insight into how to promote complete synapse repair following damaging stimuli.

• *More clearly indicate which experiments took into account the position of neuromast, as this seemed to be important in determining the extent of damage.*
We have indicated in each Figure Legend the position of the neuromasts analyzed.

• *Live cell video of macrophages engulfing HCs (and possibly other repair-related processes) would be nice and would highlight the power of the zebrafish system.*
We agree that live imaging of neuromast damage and recovery will take full advantage of the zebrafish model and is a goal of future studies. One caveat to capturing damage and repair to neuromasts in mechanically exposed larvae is paralyzing, stabilizing, and illuminating fluorescent indicators in larvae immediately following exposure induces additional stress to physically traumatized tissue, which can confound interpretation of observed pathological processes and requires careful controls and optimization. We are therefore optimizing for a future study our live-imaging protocols such that we accurately capture damage and subsequent repair following mechanical exposure.